Theoretical Calculations of Metal–Dioxygen Complexes

Ian Bytheway and Michael B. Hall*

Department of Chemistry, Texas A&M University, College Station, Texas 77843

Received February 16, 1994 (Revised Manuscript Received February 25, 1994)

Contents

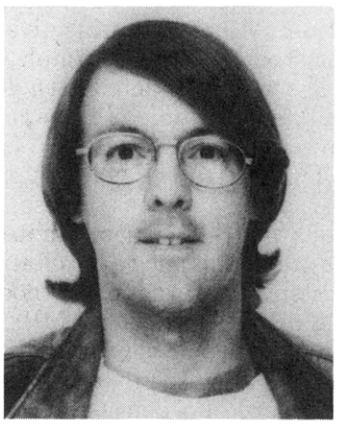

Ian Bytheway was raised in Perth, graduated from the University of Western Australia with a B.Sc. (Hons) degree in Physical and Inorganic Chemistry. He obtained a Ph.D. degree in 1991 from the same institution, under the supervision of David L. Kepert. He did postdoctoral research with Richard F. W. Bader and Ronald J. Gillespie at McMaster University during 1991 and 1992, after which he joined Michael B. Hall's research group at Texas A&M University as a Welch Foundation Postdoctoral Fellow. His main research interest is the study of molecular geometry, although he does admit to believing that all chemistry is interesting.

Michael Hall was born in Pennsylvania and graduated from Juniata College with a B.S. in Chemistry in 1966. After completing his Ph.D. at the University of Wisconsin with Richard Fenske in 1971, he accepted an Associated Electric Industries Fellowship to study *ab initio* quantum chemistry with Ian Hillier at the University of Manchester, England. In 1975, he accepted an appointment at Texas A&M University as an Assistant Professor of Chemistry. He rose through the ranks to become Associate Professor in 1980, Professor in 1983, and Professor and Head of the Department in 1986. In the Spring of 1982 he spent a sabbatical leave as an associate of Clare Hall at Cambridge University with Lord Lewis. His research interests have included transition metal complexes and organometallics, metal and nonmetal clusters, photoelectron spectroscopy, and quantum chemistry.

I. Introduction

Here we review theoretical studies of the binding of dioxygen to metal complexes published since about 1983. Reviews of theoretical calculations up to and including 1983 form an important basis upon which this work is built, and we direct the reader to these reviews for a more complete overview of previous calculations.[1-6] Calculations on iron–dioxygen complexes are reviewed in ref 1–3 and on cobalt–dioxygen complexes in ref 3 and 4, while more general reviews may be found in ref 5 and 6. Although there is considerable interest in the binding of dioxygen to metal surfaces, this subject is beyond the scope of this review. In addition, only complexes containing transition metals have been considered.[7]

Electronic structure calculations typically belong to one of three broad categories: *ab initio*, density functional, and semiempirical.[8] *Ab initio* techniques represent attempts to describe the wave function of the molecule from first principles, *i.e.*, without the incorporation of any experimental data. Equilibrium geometries of molecular ground states are often adequately described by wave functions obtained using the restricted Hartree–Fock (RHF) method for closed shell molecules and the restricted open-shell Hartree–Fock (ROHF) method for open-shell molecules. These methods are synonymous with molecular orbital calculations and provide an upper bound for the true molecular energy but are, however, inappropriate for the comparison of the relative energies of closed- and open-shell states and for the description of excited states. These situations require that electron correlation be taken into account, which may be accomplished with some variant of the configuration interaction (CI) method.

In simple CI calculations electronic configurations obtained by exciting electrons from the occupied orbitals of the reference configuration (often just the ground-state configuration) into virtual orbitals, are used to improve the overall molecular wave function. The accuracy of CI calculations may be improved by increasing both the number of reference configurations from which excitations are made and by increasing the number of electrons that are excited from the reference configurations. For example, multiple reference configuration interaction calculations including single

0009-2665/94/0794-0639$14.00/0

(excitation of one electron) and double (excitation of two electrons) excitations (MRSDCI) begin by selecting the important reference configurations obtained from a single reference CI calculation.

Configuration interaction calculations may then be implemented in a self-consistent manner as in multiconfiguration self-consistent field (MCSCF) theory where the active molecular orbitals are reoptimized for the states obtained by exciting electrons in the reference configurations. In complete active space self-consistent field (CASSCF) calculations the configurations are chosen by dividing electrons into inactive (for example, core electrons) and active (for example, valence electrons) sets. The wave function is then determined by considering all the excitations of these active electrons into a chosen set of virtual orbitals.

While all CI methods do provide an upper bound for the molecular energy, because these methods are approximations to full-CI (as some limitation has been placed on the number of allowed excitations) they are not size-consistent. Perturbation methods, such as the various levels of Møller–Plesset (MP) perturbation theory may be used if size consistency is required.

Calculation of molecular properties from first principles is also the purpose of density functional methods. Here, the energy is written as a functional of the density rather than as an eigenvalue of the wave function. Because the exact form of the functional is unknown there are many approximate versions of this approach that incorporate approximate expressions for the exchange energy (treated exactly by RHF methods) and for the correlation energy (treated exactly by full-CI). The scattered wave (Xα-SW) and the equivalent multiple scattering (MS-Xα) methods, among the simplest density functional approaches, are often used for large transition metal complexes and clusters.

In the so-called semiempirical category we would include approximate methods based on *ab initio* theory such as variations of the complete neglect of differential overlap (CNDO) methods and approximate methods, which are perhaps more closely related to density functional theory, such as extended Hückel (EH) theory and the nearly identical Mulliken–Wolfsberg–Helmholtz (MWH) method. Here, rather severe approximations are used to achieve a rapid method suitable for very large molecules. Their accuracy depends greatly on how well the methods have been tested and adjusted for the particular class of complex under study.

II. Metalloporphyrins

The metalloporphyrins are models for the active site of heme proteins which have the important biological task of carrying dioxygen. These molecules are large and their study by *ab initio* techniques requires that compromises be made in order to calculate at least some of the metalloporphyrin's properties. Although it would be preferable to treat equally all aspects of the molecule it is usual to treat either the basis set, level of electron correlation, or structure at some less than desirable level of accuracy. Calculations that include electron correlation are preferable if the relative energies of open and closed shell systems are to be compared, and so basis sets must be chosen such that they allow for a meaningful description of the system without being too large. Experimental geometries, typically obtained from crystallographic studies, are used to reduce the amount of computation required as optimization of all geometrical parameters represents an unjustifiable increase in calculational effort. Similarly, smaller model ligands are often substituted for both the porphyrin and axial ligands with the hope that the reduction in ligand size does not make the results any less meaningful.

A. Iron Porphyrins

The biological importance of the heme proteins makes the bonding between iron and dioxygen an obvious starting point to begin this discussion. Before turning our attention to the results of the calculations summarized in Table 1, however, let us first review the various descriptions of the bonding between the metal atom and the dioxygen ligand that have been developed. In keeping with previous descriptions of the electronic structures in metal–dioxygen complexes the assignment of oxidation states to atoms is done in a formal manner and is not intended to depict actual atomic charges or real electron distributions.[9,10]

In one model, the end-on FeO_2 arrangement **1** consists of low-spin Fe(II) in the lowest energy-closed shell state bound by a dative bond to a formally neutral dioxygen ligand in a singlet state.[11] Transfer of the spare pair of electrons (of π symmetry) from the iron atom results in the valence bond structure **2** which may now be formally described[12] as Fe(IV) bound to O_2^{-2}. Any

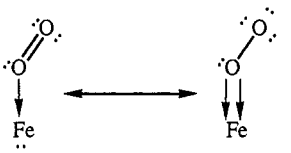

1 2

meaningful description of the bonding between iron and dioxygen must be able to account for the diamagnetism observed in hemoglobin. Here, both resonance structures are formed from closed-shell species and the observed diamagnetism is accounted for.

A bonding model consisting of Fe(III) and O_2^- arranged in an end-on manner was also proposed;[13] here both the iron atom and dioxygen ligand have an odd number of electrons. Coupling of the unpaired electrons results in a diamagnetic ground state as shown in resonance structures **3** and **4**. The bonding in this

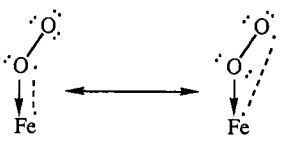

3 4

superoxide model consists of a formal Fe–O σ bond which arises from the donation of one electron pair from the dioxygen ligand and a partial π bond from the coupling of the unpaired electrons. The temperature dependence of the electric field gradient tensor obtained from Mössbauer experiments was consistent with low-spin Fe(III)[14] with spin coupling resulting in an overall diamagnetic state.

Table 1. A Summary of the Various Calculations Discussed

ref(s)	calculational details	system studied	method of calculation
4, 22, 34	double-ζ for the outer valence shells of the metal and oxygen atoms, minimal for all other atoms	$M(O_2)PL$ systems M = Fe, Co, Mn P = Model porphyrin ligand **10** L = NH_3 or imidazole (observed parameters)	GMO and CISD
25	triple-ζ for iron, double-ζ for all other atoms	$Fe(O_2)P$ system, C_s symmetry **15** P = the observed picket fence porphyrin ligand **11**	SCF and CI
26, 27	double-ζ for the outer valence shells of iron and oxygen atoms, minimal for all other atoms	$Fe(O_2)PL$ system, C_s symmetry P = the observed picket fence porphyrin ligand **11** L = NH_3 (observed parameters)	GVBCI (1985) CASSCF, 14 electrons in an active space of 11 orbitals (1989)
28	quadruple-ζ for iron, double-ζ for oxygen supplemented with extra p and d functions, double-ζ for all other atoms	$Fe(O_2)PL$ system, C_s symmetry P = the observed picket fence porphyrin ligand **11** L = imidazole (observed parameters)	CASSCF, 14 electrons in an active space of 11 orbitals
29	double-ζ for iron with an additional 4p function, minimal basis set with an extra diffuse function for all other atoms	$M(O_2)^+$ M = Fe, Cr $M(O_2)^{+2}$ M = Ni $M(O_2)(NH_2)_4$ M = Cr, Fe, Ni $M(O_2)(NH_2)_4NH_3$ M = Cr, Fe $Fe(O_2)(NH_2)_4L$ L = SH, imidazole $Fe(O_2)(NH_2)_4LH_2O$ L = NH_3, SH	UHF various closed- and open-shell states considered for each complex
30	Slater type orbitals: 3d, 4p and 4s for iron, 3s, 3p for sulfur, and 2s, 2p for carbon, nitrogen, and oxygen	$Fe(O_2)PL$ system P = the observed picket fence porphyrin ligand **11** L = imidazole, $SC_6F_4H^-$, SCH_3^- and $SHCH_3$ (observed parameters)	MO-LCAO using the MWH approximation
31	empirical parameters for fixed portions of the molecule, theoretical parameters for the dioxygen ligand	$Fe(O_2)PL$ and $FeL(O_2)\cdots H_2O$ systems **16** P = the observed picket fence porphyrin ligand **11** L = imidazole (observed parameters)	INDO
41	double-ζ basis sets with diffuse and polarization functions for the oxygen atoms and a double-ζ basis set for the copper atom	$(Cu^+)_2$–O_2 **26–31**	ROHF to construct binding curves ROHF-GVB to model geometrical parameters ROHF-GVB-CI for calculations at the optimal geometries
43		$[(NH_3)_3Cu(O_2)Cu(NH_3)_3]^{2+}$ **33, 34** $[(NH_3)_4Cu(O_2)Cu(NH_3)_4]^{2+}$ **35**	EHMO
44		$[(Im)_3Cu(O_2)Cu(Im)_3]^{2+}$ **36, 37**	EHMO
45		$[Cu(O_2)]$ *cf.* **7**	Xα-SW
47		$[ML_4(O_2)]^+$ **43** averaged observed bond lengths and angles	SCF-Xα-SW
49		$[M(O_2)_4]^{n-}$ **44** M = Cr(V), Mo(VI), and Nb(V) idealized D_{2d}, triangular dodecahedra	SCF-MS-Xα
50	double-ζ basis sets for all atoms	$[Ni(N_2)(O_2)]$ **45–47** optimized bond lengths and angles	LCAO-MO-SCF
58	triple-ζ basis sets for the metal atoms, double-ζ for carbon, nitrogen, and oxygen	$[TiL(O_2)]$ **52** L = the bidentate ligand, 2,6-pyridine-dicarboxylate $[NiL_2(O_2)]$ **53** L = methylisocyanate experimental crystal geometries used (methyl group substituted for the *tert*- butyl group of the observed molecule)	RHF
62	triple-ζ basis sets for the metal atoms, double-ζ for carbon, nitrogen, and oxygen	$[NiL_2(O_2)]$ *cf.* **53**	SCF and MRSDCI calculations at the experimental geometry
64		$[Pd(HCO_2)(O_2)]$ **57–59** $[Pd_3(HCO_2)_5(O_2)]$	semiempirical SCF-MO CNDO-S[2]

Binding of dioxygen to iron through the formation of an intermediate spin state of Fe(II) has also been suggested.[15] In this model, the bonding occurs not with an excited or ionic state of dioxygen nor with either high, **5a**, or low-spin Fe(II), **5b**, but rather, the Fe(II) is promoted to a state with intermediate spin ($S = 1$), **5c**, prior to bond formation with the ground state dioxygen ($^3\Sigma_g^-$). Thus the primary electronic reorganization occurs at the Fe(II) atom rather than the dioxygen molecule, which results in a total of four unpaired electrons. Once this reorganization of the Fe(II) electrons has occurred, coupling between the unpaired electrons on both dioxygen and iron takes

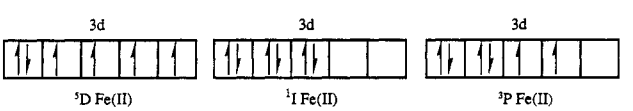

place,[16] resulting in the formation of the iron–dioxygen bond, as shown in **6**.

This spin coupling in FeO_2 is analogous to the bonding in ozone and this similarity has been used to describe the bonding between iron and dioxygen in valence bond terms[17,18] as shown in Figure 1. Here, the Fe–O σ bond is formed by coupling the singly occupied iron d_{z^2} orbital and the singly occupied dioxygen p_z orbital; the Fe–O

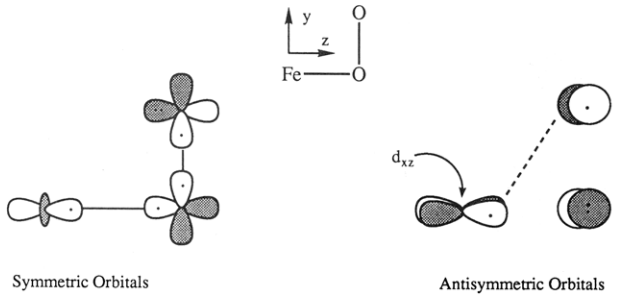

Figure 1. A valence-bond representation of the ozone-bonding model showing spin paring of electrons, for the FeO_2 part of an iron porphyrin. (Adapted from ref 17).

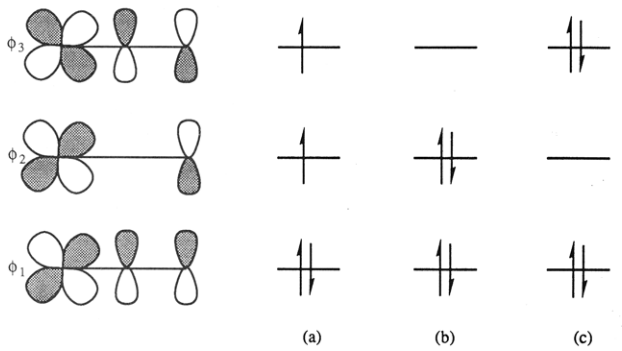

Figure 2. A MO representation of the bonding between iron and dioxygen showing the three-orbital, four-electron interaction.

π bond is formed by coupling of the single electron in the iron d_{xz} with the remaining single electron in the dioxygen p_x orbital. The four remaining electrons belonging to Fe(II) occupy the $d_{x^2-y^2}$ and d_{yz} orbitals, while the d_{xy} orbital, which is directed toward the nitrogen atoms of the porphyrin ligand, is unoccupied. Additional resonance structures are shown in **6**.

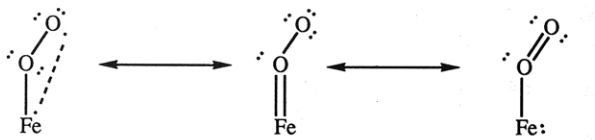

6

As in ozone, the π bonding in FeO_2 may be thought of as a three-orbital, four-electron interaction and may also be explained in qualitative MO terms by considering the three relevant MO's ϕ_1, ϕ_2, and ϕ_3 shown in Figure 2. The triplet state obtained by filling the orbitals in the manner $\phi_1^2\phi_2^1\phi_3^1$ (Figure 2a) has an energy lower than the single configuration singlet state, described by $\phi_1^2\phi_2^2\phi_3^0$ (Figure 2b). The singlet state is, however, the correct description of the ground state because when contributions from the $\phi_1^2\phi_2^0\phi_3^2$ configuration (Figure 2c), are taken into account the singlet state is lower in energy than the triplet. This is analogous to the bonding situation in ozone in which configuration interaction, *i.e.*, taking into account other possible electron configurations of the molecule, obtained by exciting two electrons into higher energy MO's, is required in order to describe the ground state of the molecule correctly. As for O_3 the necessity of this CI description of FeO_2 is a consequence of atomic orbitals having similar energies and small overlap.[4]

Crystallographic studies support the bent, end-on arrangement of the FeO_2 in heme proteins;[19] prior to the confirmation of the bent FeO_2 geometry, side-on geometries were proposed.[20,21] The bonding of the side-on geometry, which is important to the dioxygen complexes of other metals, was initially suggested to be like metal ethylenic π complexes.[20] Side-on binding of singlet dioxygen to low-spin Fe(II) may occur via overlap of the iron d and dioxygen π orbitals, as shown in **7**, with **7a** less important here. The relative arrangements of the dioxygen and porphyrin ligand is shown in **8**.

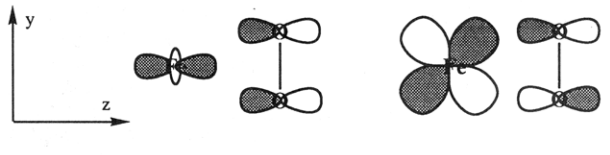

7a **7b**

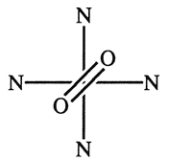

8

A side-on bonding description obtained by the oxidative addition of dioxygen to Fe(II) has also been suggested.[21] The resultant complex contains a d^4, low-spin Fe(IV) bound to both ends of the peroxide ligand, as in **9**. Note that equal iron–oxygen bond lengths are

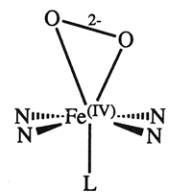

9

not necessary. The electron-donating ability of both the porphyrin and the axial imidazole ligand are important factors for the viability of this model. Consequently, this model predicts a short Fe–L bond length, along with the iron atom situated above the porphyrin plane.

A qualitative molecular orbital diagram[4] for a dioxygen ligand bound end on to a typical iron porphyrin is given in Figure 3. The higher valence orbitals of dioxygen and the iron 3d orbitals interact to produce the iron–oxygen bonding and antibonding σ_z orbitals, and the bonding and antibonding iron–oxygen π_y orbitals. The σ_z and σ_z* orbitals are formed from the interaction between the metal $3d_{z^2}$ and the in-plane, antibonding $1\pi_g^s$ orbital, where the superscript s (and a) refer(s) to whether or not the orbital is symmetric (or antisymmetric) with respect to the MO_2 plane. The π_y and π_y* orbitals are formed by the out-of-plane $1\pi_g^a$ interacting with the $3d_{yz}$ orbital. Thus a typical Fe-(O_2)PL system (where P will be used to denote the porphyrin ligand and L a ligand in the site axial to the attached dioxygen) consists of 14 electrons (six from Fe(II) and eight p electrons from dioxygen) which must be placed in the MO's shown in Figure 3; the most

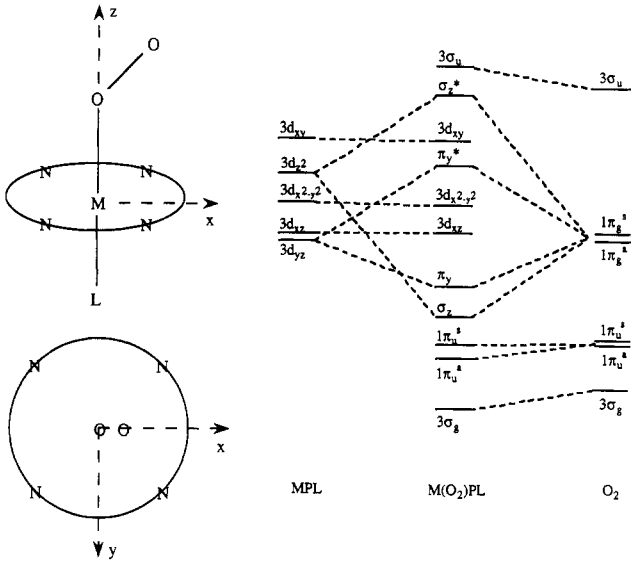

Figure 3. A qualitative molecular orbital diagram for the $M(O_2)PL$ (M = Fe or Co, P = porphyrin or model ligand, L = NH_3 or Im) molecule with the orientation of the molecule with respect to the coordinate axes shown also. The M-O_2 σ-bonding and antibonding molecular orbitals are formed from the interaction between the $3d_{z^2}$ and $1\pi_g^a$ atomic orbitals. These are labeled σ_z and σ_z^*. The π-bonding and antibonding orbitals are formed from the $3d_{yz}$ and $1\pi_g^s$ atomic orbitals, labeled π_y and π_y^* respectively. (Adapted from ref 22.)

obvious solution is to fill the $3\sigma_g$, $1\pi_u^a$, $1\pi_u^s$, σ_z, π_y, $3d_{xz}$ and $3d_{x^2-y^2}$ MO's. Occupying these orbitals in this manner may not be the only relevant possibility, and it must be kept in mind that it may be necessary to include contributions from other occupation patterns (*i.e.*, through CI) to account for the observed properties of these molecules.

The calculation of the electronic structure of a molecule containing a transition metal, a porphyrin ligand, and one or two axial ligands requires considerable computational effort. Such a calculation may be made more manageable, however, if a ligand approximating the porphyrin ring is used to reduce the number of atoms that must be considered in the calculation. This smaller ligand in turn allows for the use of larger basis sets and the use of calculational methods which take into account electron correlation. GMO-CI calculations of an $Fe(O_2)PL$ complex using the model porphyrin ligand **10** were performed by Newton and Hall[22] after this ligand was shown to give results from approximate MO calculations similar to those obtained by using the real porphyrin ligand **11**.

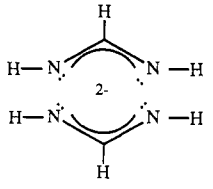

10

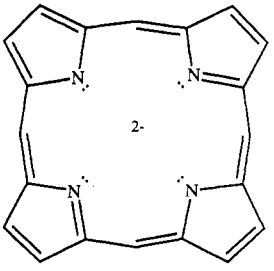

11

Other ligands were also considered in this work as possible models for the porphyrin ligand, **12** was rejected because of its inability to account for the π delocalization

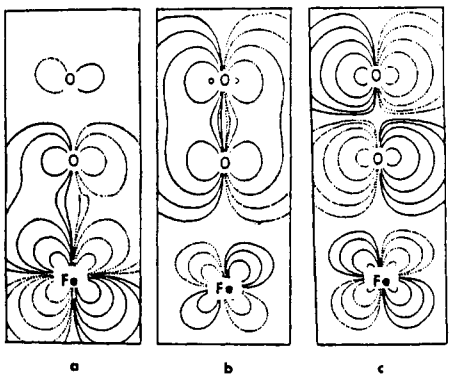

Figure 4. The FeO_2 π MO's plotted in the Fe–O–O plane projected onto the *yz* plane: (a) the bonding π_y MO showing some mixing with the dioxygen $1\pi_u^a$ orbital; (b) the out of phase mixing of the π_y and $1\pi_u^a$ orbitals; and (c) the π_y^* MO. (Reprinted from ref 22. Copyright 1984 American Chemical Society.)

in the porphyrin ring system. While this delocalization is present in **13** and **14**, **10** was chosen as it provided the best balance between size and accuracy (Table 1: entry 1).[22]

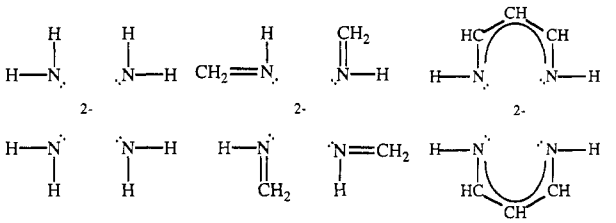

12 **13** **14**

These GMO-CI calculations, which were performed with basis sets of double-ζ quality for the iron and oxygen atoms, showed that the configuration obtained by filling the first seven orbitals of Figure 3, *i.e.*, $(3\sigma_g)^2(1\pi_u^a)^2(1\pi_u^s)^2(\sigma_z)^2(\pi_y)^2(3d_{xz})^2(3d_{x^2-y^2})^2$ accounts for 91% of the wave function. The next most important configuration, which accounts for 3% of the wave function, is obtained by the double excitation from π_y to π_y^*, *i.e.*, the excitation of the two π bonding electrons of FeO_2 into the corresponding antibonding orbital. The remainder of the wave function is made up of small contributions (less than 1%) of which the most important configurations involve single or double excitations from the π_y to the π_y^* orbital. The natural orbitals and their occupanices obtained from these calculations also show mixing between the π_y and $1\pi_u^a$ orbitals: $(3\sigma_g)^{1.96}(1\pi_u^s)^{2.00}(\pi_y+1\pi_u^a)^{1.99}(\sigma_z)^{1.99}(\pi_y-1\pi_u^a)^{1.90}(3d_{xz})^{2.00}$-$(3d_{x^2-y^2})^{2.00}(\pi_y^*)^{0.11}(3d_{xy})^{0.01}(\sigma_z^*)^{0.01}(3\sigma_u)^{0.04}$.

Plots of the π MO's are shown in Figure 4. It can be seen that the $\pi_y+1\pi_u^a$ orbital (Figure 4a) is mostly $3d_{yz}$ delocalized onto the proximal oxygen atom of the dioxygen ligand, while the $\pi_y-1\pi_u^a$ orbital (Figure 4b) is primarily the dioxygen $1\pi_u^a$ with an antibonding interaction with the iron atom. The antibonding π_y^* orbital (Figure 4c) consists of an almost equal mixture iron and the two oxygen orbitals with a node between each. This system of orbitals is analogous to the three-center, four-electron π bond discussed above for ozone.

The σ MO's are plotted in Figure 5. The Fe–O σ_z bonding orbital (Figure 5a) involves donation from a dioxygen molecular orbital (which is a mixture of $1\pi_u^s$, $1\pi_g^s$, and $3\sigma_g$ orbitals) to a hybrid iron orbital (which

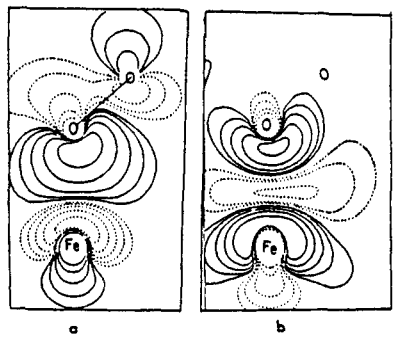

Figure 5. The FeO_2 σ MO's plotted in the xz plane: (a) the bonding σ_z MO and (b) the antibonding σ_z* MO. (Reprinted from ref 22. Copyright 1984 American Chemical Society.)

is in turn a mixture of $3d_{z^2}$, 4s, and $4p_z$ orbitals). This mixing results in the rotation and enlargement of the lobe on the oxygen atom nearest the iron center, obvious in Figure 5a. The antibonding σ orbital, as a consequence of this mixing, has the pattern of nodes shown in Figure 5b, one close to the midpoint of the Fe–O bond and one close to the iron atom.

The energy corresponding to the excitation from the ground to the first excited state was also estimated at the HF level of theory. The single determinant wave function $(\sigma_z)^2(d_{xz})^2(3d_{x^2-y^2})^2(\pi_y)^1(\pi_y^*)^1$ for the $^3A'$ state and the two-determinant wave function $(\sigma_z)^2(d_{xz})^2(3d_{x^2-y^2})^2[(\pi_y)^2+\lambda(\pi_y^*)^2]$ for the $^1A'$ state were used in order to produce energies calculated at the same level of accuracy. The energy separating these singlet and triplet states was calculated to be 850 cm^{-1}, with the $^1A'$ state being of lower energy. This value is larger than the observed[23] value of 146 cm^{-1} although this experimental result has been questioned.[24]

Calculations of closed- and open-shell $Fe(O_2)P$ molecules by Rohmer,[25] where there is no ligand in the axial position *trans* to the dioxygen ligand, also demonstrated the importance of including the effects of electron correlation. The geometry of this square pyramidal molecule is shown in **15** where it can be seen that the iron atom is not coplanar with the pyrrole nitrogen atoms of the porphyrin ligand. The complete porphyrin ligand **11** was used in these calculations with bond lengths and angles obtained from experiment. Basis sets used in these calculations were of triple-ζ quality for the iron atom and double-ζ for all others (see Table 1, entry 2).

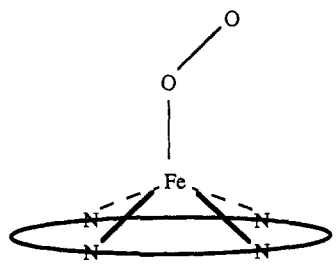

15

At the SCF level a $^3A'$ state of the model complex was found to have the lowest energy, with the next state ($^3A''$) 0.03 eV higher in energy. The lowest lying singlet state ($^1A'$) was located at 1.42 eV above the lowest triplet state. The relative orderings of these states are shown in Figure 6. The electronic configurations for each of

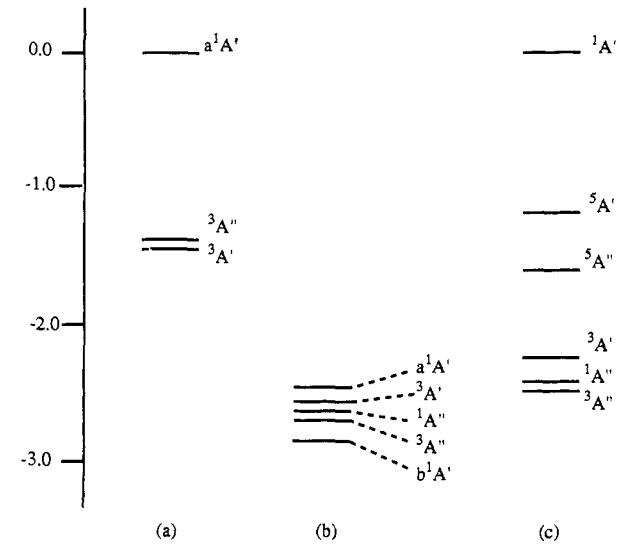

Figure 6. Calculated energies for several different states of $Fe(O_2)P$ and $Fe(O_2)PL$ molecules. The energies were adjusted so that the highest energy state has an energy of 0 eV: (a) SCF energies of the $Fe(O_2)P$ molecule,[25] (b) CI energies of the $Fe(O_2)PL$ molecule,[25] and (c) SCF energies for the $Fe(O_2)PL$ molecule.[26]

these states, using the same MO's and labeling scheme as depicted in Figure 3, are

a^1A' $(3\sigma_g)^2(1\pi_u^a)^2(1\pi_u^s)^2(\sigma_z)^2(\pi_y)^2(3d_{xz})^2(3d_{x^2-y^2})^2$,

$^3A'$ $(3\sigma_g)^2(1\pi_u^a)^2(1\pi_u^s)^2(\sigma_z)^2(\pi_y)^1(3d_{xz})^2(3d_{x^2-y^2})^2(\pi_y^*)^1$,

$^3A''$ $(3\sigma_g)^2(1\pi_u^a)^2(1\pi_u^s)^2(\sigma_z)^2(\pi_y)^2(3d_{xz})^1(3d_{x^2-y^2})^2(\pi_y^*)^1$.

CI calculations were then performed using 14 electrons in an active space of 54 orbitals. Important consequences of the inclusion of CI was the lowering of the energies of the a^1A', $^3A'$, and $^3A''$ states by significantly different amounts and the calculation of other important states. The relative orderings of the states obtained from CI calculations, from which the open-shell singlet state (b^1A') was found to have the lowest energy, are shown next to the SCF energies in Figure 6. For each of the state the configurations which contribute most to the wavefunction are

a^1A' $(3\sigma_g)^2(1\pi_u^a)^2(1\pi_u^s)^2(\sigma_z)^2(\pi_y)^2(3d_{xz})^2(3d_{x^2-y^2})^2$ (92%),

$^3A'$ $(3\sigma_g)^2(1\pi_u^a)^2(1\pi_u^s)^2(\sigma_z)^2(\pi_y)^1(3d_{xz})^2(3d_{x^2-y^2})^2(\pi_y^*)^1$ (93%),

$^1A''$ $(3\sigma_g)^2(1\pi_u^a)^2(1\pi_u^s)^2(\sigma_z)^2(\pi_y)^2(3d_{xz})^1(3d_{x^2-y^2})^2(\pi_y^*)^1$ (91%),

$^3A''$ $(3\sigma_g)^2(1\pi_u^a)^2(1\pi_u^s)^2(\sigma_z)^2(\pi_y)^2(3d_{xz})^1(3d_{x^2-y^2})^2(\pi_y^*)^1$ (90%),

b^1A' $(3\sigma_g)^2(1\pi_u^a)^2(1\pi_u^s)^2(\sigma_z)^2(\pi_y)^1(3d_{xz})^2(3d_{x^2-y^2})^2(\pi_y^*)^1$ (59%),

along with

$(3\sigma_g)^2(1\pi_u^a)^2(1\pi_u^s)^2(\sigma_z)^2(\pi_y)^2(3d_{xz})^2(3d_{x^2-y^2})^2$ (30%).

(Note that the singlet, $^1A'$ and $^1A''$, and triplet, $^3A'$ and $^3A''$, states involve the same orbitals and only differ in the spin coupling of the electrons.)

The lowest state obtained from these CI calculations involves the mixing of open- and closed-shell configurations and is qualitatively similar to that obtained from the GMO-CI calculations of Newton and Hall for the $Fe(O_2)PL$ molecule presented above.[22] In both cases the ground state is made up of contributions from the all-paired configuration as well as one obtained by the excitation of an electron from the π_y orbital into the π_y^* orbital. The difference between the GMO-CI results of Newton and Hall,[22] and the SCF-CI results of Rohmer[25] is that the b^1A' state involves strong mixing of configurations in which the open-shell singlet is dominant (59% is due to the $\pi_y \rightarrow \pi_y^*$ configuration and 30% is due to the all-paired configuration) while the state obtained from GMO-CI calculations is predominantly due to the all-paired configuration (91%). Thus the b^1A' state may be thought of as made up of a mixture of the Fe^{II}–O_2 and Fe^{III}–O_2^- descriptions of FeO_2. It should be kept in mind, however, that the two $^1A'$ states are rather close in energy and a lowering of the π_y^* orbital, through better description of this virtual orbital, may result in appreciable lowering of the a^1A' state over the b^1A' state.[25] In a more technical (less physical) view these valence descriptions depend upon the orbitals used in the CI and in a fully optimized MCSCF the importance of the single excitations will decrease enormously. Thus, the "best" MCSCF description will be dominated by configurations which differ by two electrons, *i.e.* configurations involving $(3\sigma_g)^2(1\pi_u^a)^2(1\pi_u^s)^2(\sigma_z)^2(\pi_y)^2(3d_{xz})^2(3d_{x^2-y^2})^2$ and $(3\sigma_g)^2(1\pi_u^a)^2(1\pi_u^s)^2(\sigma_z)^2(3d_{xz})^2(3d_{x^2-y^2})^2(\pi_y^*)^2$.

Calculations of $Fe(O_2)PL$ at the SCF level, where P is the porphyrin ligand 11 and L the NH_3 ligand were performed by Nozawa *et al.*[26] using a double-ζ basis set to describe iron and minimal basis sets for all the other atoms (see Table 1, entry 3). The six different states obtained are (arranged in order of decreasing SCF energy):

$^1A'$ $(3\sigma_g)^2(1\pi_u^a)^2(1\pi_u^s)^2(\sigma_z)^2(\pi_y)^2(3d_{xz})^2(3d_{x^2-y^2})^2$,

$^5A'$ $(3\sigma_g)^2(1\pi_u^a)^2(1\pi_u^s)^2(\sigma_z)^1(\pi_y)^1(3d_{xz})^2(3d_{x^2-y^2})^2(\pi_y^*)^1$-$(\sigma_z^*)^1$,

$^5A''$ $(3\sigma_g)^2(1\pi_u^a)^2(1\pi_u^s)^2(\sigma_z)^1(\pi_y)^2(3d_{xz})^1(3d_{x^2-y^2})^2(\pi_y^*)^1$-$(\sigma_z^*)^1$,

$^3A'$ $(3\sigma_g)^2(1\pi_u^a)^2(1\pi_u^s)^2(\sigma_z)^2(\pi_y)^1(3d_{xz})^2(3d_{x^2-y^2})^2(\pi_y^*)^1$,

$^1A''$ $(3\sigma_g)^2(1\pi_u^a)^2(1\pi_u^s)^2(\sigma_z)^2(\pi_y)^2(3d_{xz})^1(3d_{x^2-y^2})^2(\pi_y^*)^1$, and

$^3A''$ $(3\sigma_g)^2(1\pi_u^a)^2(1\pi_u^s)^2(\sigma_z)^2(\pi_y)^2(3d_{xz})^1(3d_{x^2-y^2})^2(\pi_y^*)^1$.

Their relative energies are also shown in Figure 6.

It is necessary that some attempt be made at estimating the correlation energy differences if the SCF energies of open- and closed-shell molecules obtained by Nozawa *et al.*[26] are to be compared. The energy differences between the singlet and the triplet and quintet states were estimated to be 2.0 and 1.2 eV, respectively. Even with these corrections the $^3A''$ state, again corresponding to Fe^{III}–O_2^-, is still of lowest energy. The Mössbauer parameters given in Table 2 indicate that other states may, however, be promising candidates for the ground state if electron correlation is included. For example, in this calculation the $^1A''$ state has the correct sign for both the QS and principal axis and, as was shown in the calculations performed by Rohmer for the $Fe(O_2)P$ molecule,[25] the inclusion of correlation may result in energy lowerings of the singlet and triplet states by different amounts.

Table 2. Observed and Calculated Mössbauer Parameters[26-28]

model	state	QS	η	direction
$Fe(O_2)PL$[a]	$^1A'$	0.65	0.5	z
	$^5A''$	−1.01	0.98	z
	$^5A'$	1.44	0.68	y
	$^1A''$[b]	−1.11	0.81	y
	$^3A''$	−1.13	0.74	y
	$^3A'$	−1.19	0.53	x
$Fe(O_2)PL$[c]	$^1A'$	−1.05	0.56	x
	$^1A''$	−0.90	0.57	$-x$
$Fe(O_2)PL$[d]	$^1A'$	−0.98	0.72	x
	$^1A''$	0.99	0.66	x
experimental $Fe(T_{piv}PP)$ (1-MeIm)O_2[e]		−2.1	0.23	x or y
oxyhemoglobin[f]		−2.24		x or y

[a] Reference 26. [b] Spin-coupled singlet state. [c] Reference 26. [e] As cited in ref 28 (Spartalian, K.; Lang, G.; Collman, J. P.; Gagne, R. R.; Read, C. A. *J. Chem. Phys.* **1975**, *63*, 5375). [f] As cited in ref 28 (Lang, G.; Marshall, W. *Proc. Phys. Soc.* **1966**, *87*, 3; Lang, G.; Marshall, W. *J. Mol. Biol.* **1966**, *18*, 385).

The effect of electron correlation was subsequently studied by Yamamoto and Kashiwagi who performed CASSCF calculations[27] (Table 1, entry 3) with the same geometrical parameters and basis sets as those used in the SCF calculations of Nozawa *et al.*[26] In these CASSCF calculations the same 14 electrons were distributed in all possible ways among the orbitals in the active space consisting of the 11 MO's, shown in Figure 3. As found in the CI calculations of Rohmer,[25] the CASSCF calculations resulted in a different ordering of states compared to those obtained from the initial SCF calculations. The two lowest energy states for which CASSCF wave functions were obtained were the $^1A'$ and $^1A''$ states, of which only the former gave Mössbauer parameters in rough agreement with experiment. In contrast to the SCF results, CASSCF calculation of the $^1A''$ state did not give the correct sign and direction for the principal component of the electric field gradient tensor (see Table 2). The dominant configurations of the $^1A'$ state are

$(3\sigma_g)^2(1\pi_u^a)^2(1\pi_u^s)^2(\sigma_z)^2(\pi_y)^2(3d_{xz})^2(3d_{x^2-y^2})^2$ (64%),

$(3\sigma_g)^2(1\pi_u^a)^2(1\pi_u^s)^2(\sigma_z)^2(3d_{xz})^2(3d_{x^2-y^2})^2(\pi_y^*)^2$ (13%),

$(3\sigma_g)^2(1\pi_u^a)^2(1\pi_u^s)^2(\sigma_z)^1(\pi_y)^1(3d_{xz})^2(3d_{x^2-y^2})^2(\pi_y^*)^1(\sigma_z^*)^1$ (6%),

$(3\sigma_g)^2(1\pi_u^a)^2(1\pi_u^s)^2(\pi_y)^2(3d_{xz})^2(3d_{x^2-y^2})^2(\sigma_z^*)^2$(3%), and

$(3\sigma_g)^2(1\pi_u^a)^2(1\pi_u^s)^2(3d_{xz})^2(3d_{x^2-y^2})^2(\pi_y^*)^2(\sigma_z^*)^2$ (3%).

The major contribution to the wave function corresponds to the resonance structures **1** and **2**, with important contributions from other configurations.

The CASSCF orbital occupation numbers obtained from these calculations were $(3\sigma_g)^{1.96}(1\pi_u^a)^{1.98}(1\pi_u^s)^{1.96}$-$(\sigma_z)^{1.78}(\pi_y)^{1.57}(3d_{xz})^{1.95}(3d_{x^2-y^2})^{1.97}(\pi_y^*)^{0.50}(3d_{xy})^{0.05}$-$(\sigma_z^*)^{0.25}(3\sigma_u)^{0.04}$ which reflects the large amount of

configuration mixing in the CASSCF wave function. The most significant difference between the SCF[26] and CASSCF[27] results is that with the inclusion of electron correlation, the occupation of the σ_z and π_y orbitals has decreased while the occupation of the π_y^* and σ_z^* orbitals has increased.

Although these CASSCF calculations of Yamamoto and Kashiwagi[27] demonstrate the importance of including electron correlation, they were carried out using rather small basis sets, and thus these results (at least in a quantitative sense) may be questioned. In order to obtain more accurate results, these authors[28] performed CASSCF calculations with larger basis sets: quadruple-ζ for iron; double-ζ supplemented by p and d functions for oxygen and double-ζ for carbon, nitrogen, and hydrogen (see Table 1, entry 4). Additionally, an imidazole, instead of an ammonia, ligand was placed in the axial position opposite the dioxygen ligand making the model complex more like the real heme active site.

The $^1A'$ state was again calculated to be of lower energy than the $^1A''$ state, by 0.705 eV, and as with their previous[27] CASSCF calculations, the $^1A''$ state gave incorrect Mössbauer parameters. The dominant configurations of the $^1A'$ wave function were found to be

$$(3\sigma_g)^2(1\pi_u^a)^2(1\pi_u^s)^2(\sigma_z)^2(\pi_y)^2(3d_{xz})^2(3d_{x^2-y^2})^2 \ (68\%),$$

$$(3\sigma_g)^2(1\pi_u^a)^2(1\pi_u^s)^2(\sigma_z)^2(3d_{xz})^2(3d_{x^2-y^2})^2(\pi_y^*)^2 \ (10\%),$$

$$(3\sigma_g)^2(1\pi_u^a)^2(1\pi_u^s)^2(\sigma_z)^1(\pi_y)^1(3d_{xz})^2(3d_{x^2-y^2})^2(\pi_y^*)^1(\sigma_z^*)^1 \quad (5\%),$$

$$(3\sigma_g)^2(1\pi_u^a)^2(1\pi_u^s)^2(3d_{xz})^2(3d_{x^2-y^2})^2(\pi_y^*)^2(\sigma_z^*)^2 \ (2\%),$$

$$(3\sigma_g)^2(1\pi_u^a)^2(1\pi_u^s)^2(\pi_y)^2(3d_{xz})^2(3d_{x^2-y^2})^2(\sigma_z^*)^2 \ (2\%), \text{ and}$$

$$(3\sigma_g)^2(1\pi_u^a)^2(1\pi_u^s)^2(\sigma_z)^1(\pi_y)^1(3d_{xz})^2(3d_{x^2-y^2})^2(\pi_y^*)^1(\sigma_z^*)^1 \quad (2\%).$$

The dominant configuration is similar to that found in Yamamoto and Kashiwagi's previous CASSCF calculations,[27] where this configuration made a contribution of 64% to the wave function. The second-most important configuration corresponds to the excitation of two electrons from the π_y to π_y^* orbital. Note also that the third and sixth of these configurations differ not in occupancy but in spin coupling, as both are open-shell singlets. The CASSCF orbital occupancies obtained from the $^1A'$ wave function are $(3\sigma_g)^{1.96}(1\pi_u^a)^{1.98}(1\pi_u^s)^{1.95}(\sigma_z)^{1.79}(\pi_y)^{1.63}(3d_{xz})^{1.97}(3d_{x^2-y^2})^{1.98}(\pi_y^*)^{0.43}(3d_{xy})^{0.04}(\sigma_z^*)^{0.23}(3\sigma_u)^{0.04}$ which is once again a reflection of the contributions made by the dominant configurations to the molecular wave function.

The relationship between the structure and reactivity of metal–dioxygen complexes was studied at the UHF level using the model porphyrin ligand **12** with a variety of metal atoms and axial ligands[29] (Table 1, entry 5). Dioxygen charge was correlated with the amount of charge transferred to the $(MO_2)^{2+}$ core which resulted in three clusters of points, described as having weak, intermediate, or strong superoxide character depending upon the amount of this charge transferred from the ligand to the $(MO_2)^{2+}$ core. Each cluster of points reflects the type of P–L combination used in the calculation. The naked $(MO_2)^{2+}$ molecules were characterized as weak superoxide systems, the molecules having an axial ligand coordinated through a nitrogen atom were characterized as intermediate superoxide systems, and molecules having an axial, anionic thiol ligand were characterized as strong superoxide systems. An increase in superoxide character is a consequence of the fact that more charge from the P and L ligands is available for transfer, which in turn affects the reactivity of the molecule. It should be noted, however, that these calculated net atomic charges depend upon the level of calculation performed, and further study bearing this in mind should be carried out.

Calculations of cytochrome P450 models, *i.e.*, Fe-(O_2)PL where L is coordinated to iron through a sulfur atom, using the MWH approximation have also been reported[30] (Table 1, entry 6). The ground state obtained from these calculations was also a singlet, with more negative charge on the dioxygen ligand in this case compared to similar calculations where L is coordinated through a nitrogen atom. This result is essentially the same as that presented in the preceding paragraph, *i.e.*, that the number and type of other ligands coordinated to the iron center are important in understanding the reactivity of dioxygen complexes.

Semiempirical methods reduce significantly the amount of calculational effort required to study metalloporphyrins and consequently allows for optimization of the molecular geometry. A partial geometry optimization of an Fe(O_2)PL complex, in which porphyrin and ligand parameters were fixed while those of dioxygen parameters were varied, was performed at the semiempirical, INDO level of theory[31] (Table 1, entry 7). Two minima corresponding to the end-on and side-on isomers were located, with the interesting result that the side-on isomer is lower in energy than the end-on isomer by 2.7 kcal mol^{-1}.

Further calculations were also performed at this level taking into account the interaction of the bound dioxygen ligand with a water molecule in order to mimic the interaction of the dioxygen ligand with an amino acid residue. Upon introduction of hydrogen-bonding interactions in this manner, the "kinked" end-on isomer **16** was obtained and no minimum corresponding to the side-on coordination of dioxygen was located. This

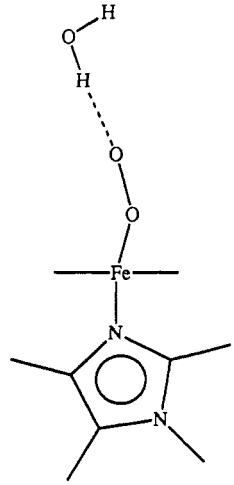

16

stabilization of the end-on geometry through the formation of intermolecular hydrogen bonding may be

an important factor affecting the mode of dioxygen coordination in biological systems. While semiempirical methods may provide some insight into possible coordination modes and geometries, these results must be considered in light of the fact that calculations utilizing large basis sets and including electron correlation are required for an accurate description of iron–dioxygen bonding.

What is clear from all of the calculations discussed in this section is that obtaining a description of the bonding in dioxygen in iron porphyrins is not simple. The importance of both basis set size and electron correlation is evident from the *ab initio* calculations discussed in this section. GMO-CI calculations with a model porphyrin ligand[4,22] resulted in the Fe^{II}–O_2 description, while other calculations in similar-sized basis sets with SCF-CI[25] and SCF[26] methods were dominated by the open-shell Fe^{III}–O_2^- description (but with substantial contribution from the closed-shell Fe^{II}–O_2 description). CASSCF calculations[27,28] with both small and large basis sets gave a wave function again dominated by the closed-shell configuration but with larger contributions from doubly excited configurations than the GMO-CI calculations.[4,22] Thus, it would seem for any reasonable description of the iron–dioxygen bonding that electron correlation is essential.

Although the exact balance between the contributions of the open-, and closed-shell configurations may change slightly as calculations are improved, this change will probably not result in a significantly new description of the bonding between iron and oxygen in these complexes. The challenge now is to use the appropriate level of theory to answer chemical questions about these complexes. For example, what is the effect of different axial ligands other than ammonia or imidazole? How large is the dioxygen rotation barrier and how is this affected by the presence of solvent molecules? These questions require a change of focus, that theory be used to further our understanding of heme complexes by considering other questions not directly related to the bonding between iron and oxygen.

B. Cobalt and Manganese Porphyrins

The geometry of the dioxygen ligand in cobalt porphyrins is known to be end on and the MO diagram shown in Figure 3 may again be used to describe the interactions between the cobalt d and p electrons of dioxygen. There are now 15 electrons to be placed in these orbitals (*i.e.*, one more than the analogous iron molecule) which results in the single occupation of the π_y^* orbital. Since the molecule has an extra electron it may be probed by ESR spectroscopy, from which it is known that this electron resides mainly on the dioxygen, thus the π_y^* orbital must be almost pure π_g^a and the π_y orbital mainly $3d_{yz}$. The argument concerning the nature of Co–O bonding must then center about the nature of the σ_z molecular orbital.[4]

There are four possible descriptions of the bonding of dioxygen to cobalt[4,22] depending upon how the cobalt and dioxygen orbitals interact to form the σ_z MO. If the contributions to this orbital come mainly from the dioxygen ligand the bond may be viewed as dative, for example, $Co^{3+} \leftarrow O_2^-$, and does not necessarily require the participation of lower energy π_u and σ_g dioxygen orbitals. If, however, such participation occurs a rehybridized dative bond may be formed. On the other hand, if the σ_z orbital consists of an almost equal mixture of cobalt $3d_{z^2}$ and dioxygen π_g orbitals then the system may be viewed as Co^{2+}–O_2. A strong interaction results in a bond which may be described as covalent, while a weak interaction may be described as spin coupled. CI is a useful probe in the study of the Co^{2+}–O_2 system and can be used to decide between these possibilities.

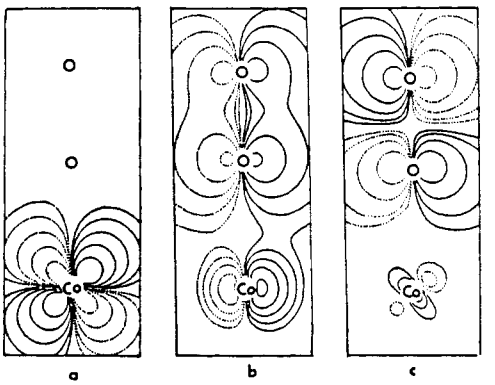

Figure 7. The CoO_2 π MO's plotted in the same plane as Figure 3: (a) the nearly pure cobalt $3d_{yz}$ orbital, (b) the nearly pure dioxygen $1\pi_u^a$ orbital, and (c) the nearly pure dioxygen $1\pi_g^a$ orbital. (Reprinted from ref 22. Copyright 1984 American Chemical Society.)

The porphyrin model ligand **10** was used in a GMO-CI calculation of a cobalt–dioxygen complex,[22] the configuration $(3\sigma_g)^2(1\pi_u^a)^2(1\pi_u^s)^2(\sigma_z)^2(\pi_y)^2(3d_{xz})^2(3d_{x^2-y^2})^2(\pi_y^*)^1$ represented 94% of the wave function with no other important configurations. The orbital occupancies obtained from these calculations were $(3\sigma_g)^{1.96}(1\pi_u^s+\sigma_z)^{2.00}(1\pi_u^a)^{1.99}(1\pi_u^s-\sigma_z)^{1.97}(3d_{yz})^{1.99}(3d_{xz})^{2.00}(3d_{x^2-y^2})^{1.99}(\pi_g^a)^{1.0}(3d_{xy})^{0.02}(\sigma_z^*)^{0.03}(3\sigma_u)^{0.04}$. Figure 7 shows the lack of mixing between the cobalt and oxygen π orbitals, resulting in almost pure $3d_{yz}$, $1\pi_u^a$ and π_g^a orbitals. The σ orbital interactions are shown in Figure 8. The nonbonding $3\sigma_g$ orbital is shown in Figure 8a and the unoccupied Co–O_2 antibonding orbital (mostly $3d_z$ in character) is shown in Figure 8d. The bonding interactions which result from mixing of $3d_{z^2}$ 4s and $4p_z$ with $1\pi_u^s$ and $1\pi_g^s$ are shown in Figure 8, parts b and c, respectively.

These results are in agreement with those obtained experimentally,[32] that the unpaired electron resides on the dioxygen ligand. Linear combinations of the bonding σ orbitals (Figure 8, parts b and c) result in the formation of a σ bond (sum) and a lone pair on the distal oxygen atom (difference). Thus the Co–O bond is essentially the donation of an oxygen lone pair to the cobalt atom, *i.e.*, the formation of a rehybridized dative bond.

On the basis of experimental data[33] the side-on coordination of dioxygen to manganese is probable, corresponding formally to Mn^{4+}–O_2^{2-} with no unpaired spin on the dioxygen ligand. Complexes of the type Mn(O_2)P contain three unpaired electrons all of which must belong to the manganese atom and singly occupy the $d_{x^2-y^2}$, d_{xz}, and d_{yz} orbitals. Previous RHF calculations[1] resulted in an end-on geometry with an unpaired electron on the dioxygen ligand—contrary to experimental results. This is not surprising as we have already seen the importance of CI for the proper description of the bonding in iron porphyrins, and the same is likely to be true for the analogous manganese complexes.

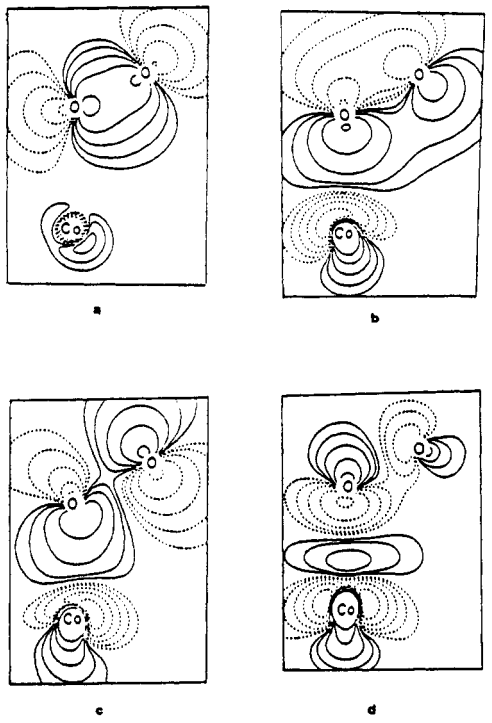

Figure 8. The CoO_2 σ MO's plotted in the xz plane: the $3\sigma_g$ orbital, (b) the cobalt σ hybrid mixing with the dioxygen $1\pi_u^s$ orbital, (c) the cobalt σ-hybrid mixing with the dioxygen $1\pi_g^s$ orbital, and (d) interaction between the cobalt $3d_{z^2}$ orbital with a mixture of dioxygen $1\pi_u^s$ and $1\pi_g^s$ orbitals. (Reprinted from ref 22. Copyright 1984 American Chemical Society.)

GMO-CI calculations for various end- and side-on orientations of the dioxygen ligand in the $Mn(O_2)P$ complex (**17**–**19**), where **10** was again used to represent the porphyrin ligand[34] (Table 1, entry 1). Initial ROHF calculations of the high-spin states of **17**–**19**, where the five Mn 3d and two dioxygen $1\pi_g$ electrons were unpaired, resulted in **17** being most stable, by over 60 kcal mol^{-1}. Experimental results suggest, however, that the ground state of the manganese porphyrin contains only three unpaired electrons, and it was for these states that CI calculations were performed. The relative energies of these RHF and GMO-CI calculations are given in Table 3.

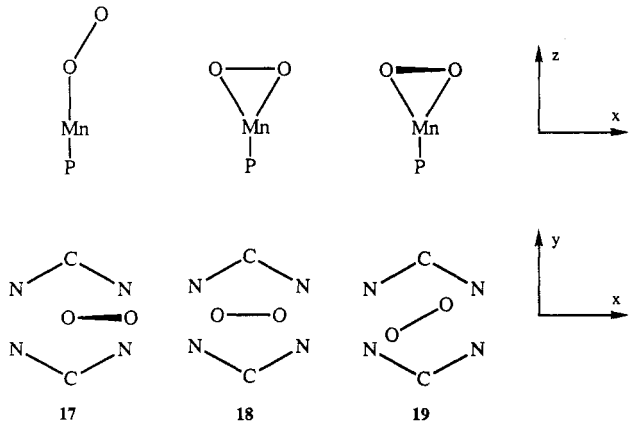

17 **18** **19**

At the RHF-CI level, *i.e.*, where the CI calculation was performed after obtaining the orbitals optimized for the octet state, the end-on geometry **17** was favored. A GMO calculation was then performed in order to reoptimize the MO's for the quartet states of **17** and **19**;

Table 3. Energies (in au) for the RHF-CI and GMO-CI Calculations[34] for the Various States of the Manganese Porphyrins 17–19

calculation	17	18	19
RHF ($S = {}^7/_2$)	$^8A''$ −1581.011	$^4B_2$ −1580.915	^8B −1580.908
CI ($S = {}^3/_2$)	$^4A'$ −1580.951	$^4A_1$ −1580.904	^4A −1580.853
	$^4A''$ −1581.034	$^4A_2$ −1580.830	^4B −1580.957
		$^4B_1$ −1580.839	
		$^4B_2$ −1580.905	
GMO ($S = {}^3/_2$)	$^4A''$ −1580.857		^4B −1580.900
CI ($S = {}^3/_2$)	$^4A''$ −1581.007		^4B −1580.978

this reoptimization resulted in **19** being of lower energy than **17**. A subsequent CI calculation, in which the five manganese 3d and two oxygen $1\pi_g$ electrons were distributed in all possible ways among the seven MO's, resulted in **17** being of lower energy than **19**. Thus, although the end-on geometry appears favorable on the basis of GMO-CI calculations, neither of the two geometries was consistently favored over the other (see Table 3).

The dominant contributions to the $^4A''$ ground state wave function of **17** were

$$(3d_{z^2}+1\pi_g^s)^2(3d_{yz}+1\pi_g^a)^2(3d_{xz})^1(3d_{x^2-y^2})^1(3d_{xy})^1\ (34\%),$$

$$(3d_{z^2}+1\pi_g^s)^2(3d_{yz}+1\pi_g^a)^1(3d_{xz})^1(3d_{x^2-y^2})^1(3d_{xy})^1\text{-}(3d_{yz}-1\pi_g^a)^1\ (19\%),$$

$$(3d_{z^2}+1\pi_g^s)^1(3d_{yz}+1\pi_g^a)^1(3d_{xz})^1(3d_{x^2-y^2})^1(3d_{xy})^1\text{-}(3d_{yz}-1\pi_g^a)^1(3d_{z^2}-1\pi_g^s)^1\ (10\%),$$

$$(3d_{z^2}+1\pi_g^s)^1(3d_{yz}+1\pi_g^a)^2(3d_{xz})^1(3d_{x^2-y^2})^1(3d_{xy})^1\text{-}(3d_{z^2}-1\pi_g^s)^1\ (9\%),$$

$$(3d_{yz}+1\pi_g^a)^2(3d_{xz})^1(3d_{x^2-y^2})^1(3d_{xy})^1(3d_{z^2}-1\pi_g^s)^2\ (4\%),\ \text{and}$$

$$(3d_{z^2}+1\pi_g^s)^1(3d_{xz})^1(3d_{x^2-y^2})^1(3d_{xy})^1(3d_{yz}-1\pi_g^a)^2\text{-}(3d_{z^2}-1\pi_g^s)^1\ (4\%).$$

These orbitals may be related to those in Figure 3 as the σ_z and π_y orbitals correspond to $3d_{z^2}+1\pi_g^s$ and $3d_{yz}+1\pi_g^a$ while the σ_z^* and π_y^* orbitals, and the correspond to $3d_{z^2}-1\pi_g^s$ and $3d_{yz}-1\pi_g^a$ respectively. The $3\sigma_g$, $1\pi_u^a$ and $1\pi_u^s$ orbitals of Figure 3 are each doubly occupied. The natural orbital occupations obtained for **17** from this calculation were $(3d_{z^2}+1\pi_g^s)^{1.62}$-$(3d_{yz}+1\pi_g^a)^{1.38}(3d_{xz})^{1.00}(3d_{x^2-y^2})^{1.00}(3d_{xy})^{1.00}(3d_{yz}-1\pi_g^a)^{0.62}$-$(3d_{z^2}-1\pi_g^s)^{0.38}$.

The results of these GMO-CI calculations suggest that the orbitals were not significantly improved over those obtained from the high-spin RHF calculations. The most dominant configuration, which correpsonds to the double occupation of both the Mn–O σ- and π-bonding orbitals, contributes only 34% to the total wave function. Double excitations from these orbitals to their antibonding counterparts, corresponding to spatial separation of the σ- and π-bonding electron pairs, make up 27%. Single excitations into these orbitals contribute 29% to the wave function. These results do show, however, that nearly all of the spin density remains on the manganese atom as the $3d_{xz}$, $3d_{x^2-y^2}$, and $3d_{xy}$ orbitals all remain singly occupied in the dominant configurations shown above. The large occupation of the antibonding orbitals is due to the inadequacy of a

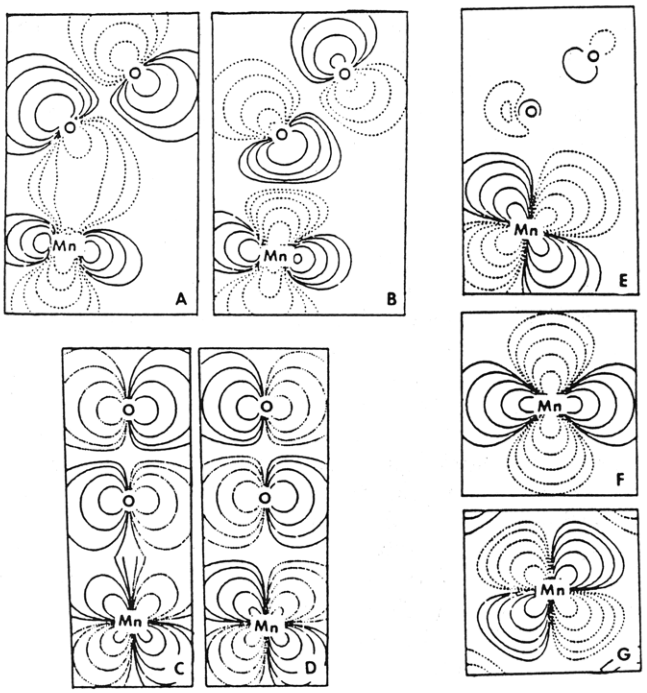

Figure 9. Plots of the natural orbitals for the $^4A''$ state of the end-on $Mn(O_2)PL$ molecule: (a) the Mn–O_2 σ-bonding MO plotted in the xz plane, (b) the Mn–O_2 σ-antibonding MO plotted in the xz plane, (c) the Mn–O_2 π-bonding MO plotted in the yz plane, (d) the Mn–O_2 π^* bonding MO plotted in the yz plane, (e) the singly occupied Mn $3d_{xz}$ orbital, (f) the singly occupied Mn $3d_{x^2-y^2}$ orbital, and (g) the singly occupied Mn $3d_{xy}$ orbital. (Reprinted from ref 34. Copyright 1985 American Chemical Society.)

simple orbital picture for this state. Plots of the MO's for **17** are shown in Figure 9, in which the lack of manganese and dioxygen orbital mixing may be seen in the singly occupied metal orbitals.

MO's for the GMO-CI calculation for the ^4B state of the side-on-coordinated dioxygen–manganese complex **19** were constructed from the in-phase combination of oxygen $1\pi_g$ orbitals with the metal 3d orbitals. In this complex the dioxygen ligand was rotated by 45° and so bisects the x and y axes, thus the contributions from the $3d_{xz}$ and $3d_{yz}$ orbitals mix to form $3d_{xz+yz}$ and $3d_{xz-yz}$ and are denoted $3d_{xz'}$ and $3d_{yz'}$ for the sake of convenience. The resultant bonding and antibonding orbitals for complex **19** after the GMO calculation are shown in **20**–**23**. Upon optimization, the δ and δ^* orbitals (**21** and **23**) rotated into a σ and σ^* set of orbitals (**24** and **25**), as a result of interactions between the $1\pi_u^s$ and $3d_{z^2}$ orbitals. During the course of the orbital optimization the $1\pi_g^a$ replaced the $1\pi_u^s$ in the doubly occupied shell and the $3d_{x^2-y^2}$ replaced the $3d_{xy}$ in the singly occupied shell. The MO diagram for this set of optimized orbitals is given in Figure 10.

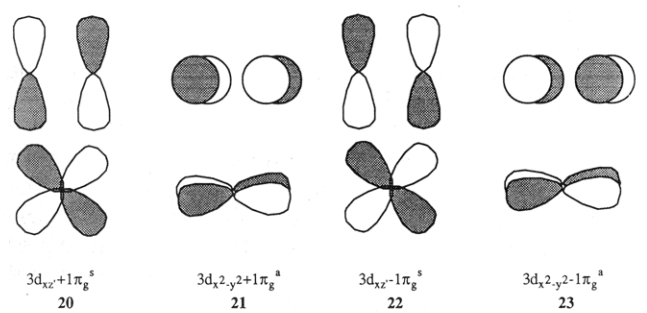

$3d_{xz'}+1\pi_g^s$ **20** $3d_{x^2-y^2}+1\pi_g^a$ **21** $3d_{xz'}-1\pi_g^s$ **22** $3d_{x^2-y^2}-1\pi_g^a$ **23**

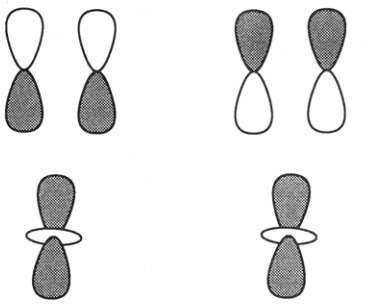

$3d_{z^2}+1\pi_u^s(\sigma)$ **24** $3d_{z^2}-1\pi_u^s(\sigma^*)$ **25**

The dominant contribution to the wave function, in contrast to that found for the end-on geometry, appears more like a ground state with the primary configuration accounting for the majority of the wave function. The most important configurations for this ^4B ground state of **19**, where the $3\sigma_g$, $1\pi_u^a$, and $1\pi_g^a$ orbitals of Figure 10 are doubly occupied in all configurations, are

$$(3d_{z^2}+1\pi_u^s)^2(3d_{xz'}+1\pi_g^s)^2(3d_{z^2}-1\pi_u^s)^1(3d_{yz'})^1(3d_{x^2-y^2})^1 \quad (73\%),$$

$$(3d_{z^2}+1\pi_u^s)^2(3d_{xz'}+1\pi_g^s)^1(3d_{z^2}-1\pi_u^s)^1(3d_{yz'})^1(3d_{x^2-y^2})^1\text{-}(3d_{xz'}-1\pi_g^s)^1 \quad (11\%),$$

$$(3d_{z^2}+1\pi_u^s)^2(3d_{z^2}-1\pi_u^s)^1(3d_{yz'})^1(3d_{x^2-y^2})^1(3d_{xz'}-1\pi_g^s)^2 \quad (7\%),$$

$$(3d_{z^2}+1\pi_u^s)^1(3d_{xz'}+1\pi_g^s)^1(3d_{z^2}-1\pi_u^s)^1(3d_{yz'})^1(3d_{x^2-y^2})^1\text{-}(3d_{z^2}-1\pi_u^s)^1(3d_{xz'}-1\pi_g^s)^1 \quad (5\%), \text{ and}$$

$$(3d_{xz'}+1\pi_g^s)^2(3d_{z^2}-1\pi_u^s)^1(3d_{yz'})^1(3d_{x^2-y^2})^1(3d_{xz'}-1\pi_g^s)^2 \quad (1\%).$$

The natural orbital occupancies also reflect the importance of the primary configuration $(3d_{z^2}+1\pi_u^s)^{1.93}\text{-}(3d_{xz'}+1\pi_g^s)^{1.75}(3d_{z^2}-1\pi_u^s)^{1.00}(3d_{yz'})^{1.00}(3d_{x^2-y^2})^{1.00}(3d_{xz'}-1\pi_g^s)^{0.27}(3d_{xy})^{0.05}$ which contrasts the results for the $^4A''$ ground state of the end-on geometry, as there is now less mixing with the antibonding orbitals. The orbitals involved in the Mn–O_2 π bond form a pair of natural orbitals due to the large amount of transfer from the $3d_{xz'}+1\pi_g^s$ orbital to its antibonding counterpart, the $3d_{xz'}-1\pi_g^s$ orbital. The MO diagram of Figure 10 shows the δ-type interaction of **21** and **23** does not occur, and this rules out the possibility of describing the system as a spin-paired side-on geometry. Plots of the natural orbitals are given in Figure 11, which show clearly the mixing to form the σ and π orbitals (Figure 11a–d) along with the singly occupied manganese d orbitals (Figure 11e–g).

Calculations for both the end-on and side-on geometries of the $Mn(O_2)P$ complex resulted in electronic configurations where three unpaired electrons reside on the manganese atom, which is in accordance with experiment. Neither of the two geometries, however, was found to be energetically preferred in all of the calculations performed. Given the poor ground-state representation of the end-on geometry, even though it is lower in energy than the side-on geometry by 18 kcal

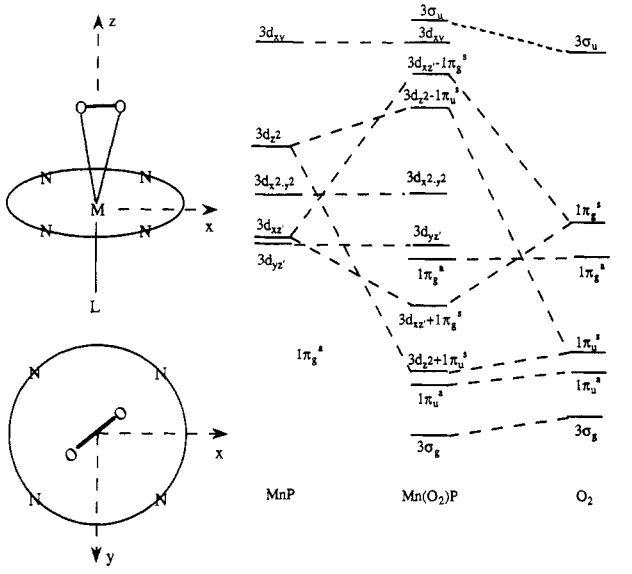

Figure 10. A qualitative molecular orbital diagram for the side-on geometry of $Mn(O_2)PL$ (**19**) showing the change in MO labeling due to the rotation of the dioxygen ligand relative to the porphyrin ring.

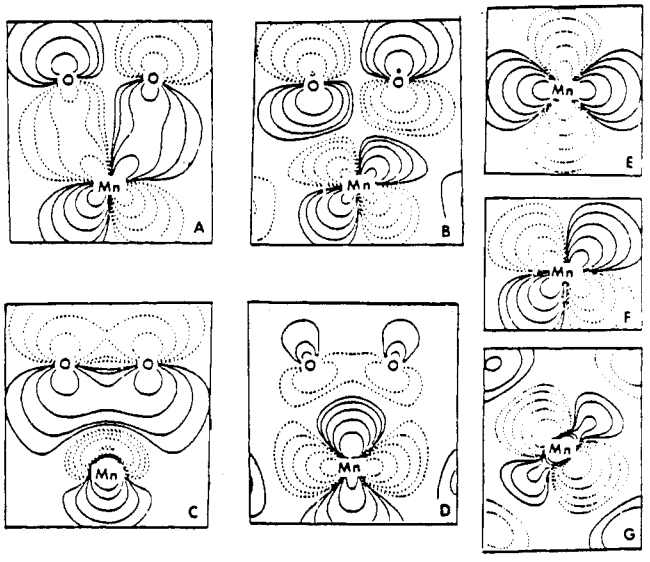

Figure 11. Plots of the natural orbitals for the ^4B state of the side-on $Mn(O_2)PL$ molecule: (a) the π-bonding combination of the Mn and O_2 plotted in the MnO_2 plane, (b) the weakly occupied antibonding counterpart of a, (c) the bonding interaction between the $3d_{z^2}$ and dioxygen $1\pi_u^s$ orbital, (d) the singly occupied nonbonded $3d_{z^2}$–$1\pi_u^s$ orbital, (e) the singly occupied manganese $3d_{x^2-y^2}$ orbital, (f) the singly occupied manganese $3d_{yz'}$ orbital, and (g) the weakly occupied manganese $3d_{xy}$ orbital. (Reprinted from ref 34. Copyright 1985 American Chemical Society.)

mol^{-1}, the side-on geometry would seem to be the preferred candidate for the structure of the $Mn(O_2)P$ complex. Larger calculations, perhaps analogous to the CASSCF calculations performed for the iron porphyrins,[28] may resolve the difficulties in describing the bonding between manganese and dioxygen in these complexes.

III. Copper–Dioxygen Complexes

The binding of dioxygen to copper is also an important bioinorganic process although less is known about the real geometry at the active sites in these molecules than in the various metalloporphyrins, although the presence of two copper atoms at the active site has been established.[35] Consequently, calculations of these complexes have been performed for various model systems, the results of which may then compared with known experimental results (*e.g.*, spectroscopic data). These model systems must, however, be chosen with some care as the requirement of including two copper atoms increases the computational effort required.

The majority of the calculations performed for dicopper–dioxygen complexes have been done using SCF-Xα-SW theory[36–40] as this allows for the study of these larger molecules without the need for prohibitive computational resources. The results of these calculations are discussed in this issue of *Chemical Reviews*,[40] and we shall refer to this when necessary rather than review the work again. Important conclusions from these studies are the description of copper–dioxygen bonding in terms of a strong dioxygen σ-donor interaction and back-bonding interactions involving the σ^* orbital of the dioxygen.[38]

Ab initio calculations of the bare dicopper–dioxygen complexes[41] **26–29** provide a means of comparing results with those obtained from SCF-Xα-SW calculations.[36–40] The four $(Cu^+)_2O_2$ complexes were studied using a 3-21G basis set supplemented with polarization and diffuse functions for oxygen and a modified 3-21G basis set was used for copper (see Table 1, entry 8). Geometries were optimized at the RHF level and the energy minima were subsequently studied by CI.

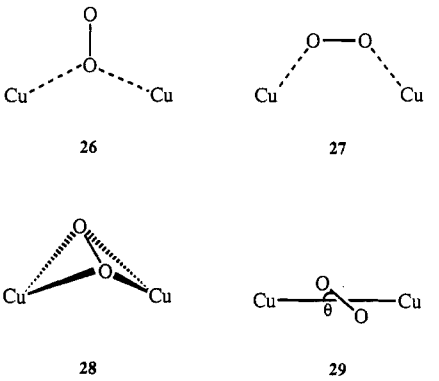

26 **27** **28** **29**

The results of the geometry optimization are shown in Figure 12, in which the variation in energy with the change in distance between the Cu–Cu and O–O midpoints (d) has been plotted for complexes **26** and **27**. In each plot two curves are shown, labeled σ and π. The σ curve corresponds to the case where the $1\pi_g^s$ orbtial is doubly occupied (*i.e.*, corresponding to a copper–oxygen σ bond). The π curve is for the case when the $1\pi_{ga}$ orbital is doubly occupied instead, leaving the $1\pi_g^s$ orbital empty. In both complexes the π configuration is preferred at low values of d until about 1.8 Å after which the σ configuration is preferred. The most favorable of these arrangements occurs when the dioxygen ligand is between the two copper atoms as shown by **29**. Further lowering of the energy occurs if the angle θ is reduced from 90° to 80°.

CI calculations were then performed for open- and closed-shell states of the optimized *cis* (**30**) and *trans* (**31**) geometries. The energies of the different states obtained from the CI calculations for **30** and **31** are given in Table 4. All single and double excitations were included in the CI calculations, the active space

Table 4. Energies (in au) of the Various Calculations[41] Performed for the $[(Cu^+)_2O_2]$ Molecules 30 and 31

	cis conformation 30			*trans* conformation 31		
	closed-shell singlet	open-shell singlet	triplet	closed-shell singlet	open-shell singlet	triplet
RHF	-3409.7941	-3409.6105	-3409.7532	-3409.8082	-3409.5347	-3409.8919
RHF-CI	-3409.8335	-3409.7689	-3409.7827	-3409.9351	-3409.8771	-3409.9203
ROHF-GVB	-3409.8905	-3409.7758	-3409.8902	-3410.0209	-3410.0181	-3410.0188
ROHF-GVB-CI	-3409.9036	-3409.8672	-3409.9024	-3410.0229	-3410.0224	-3410.0207

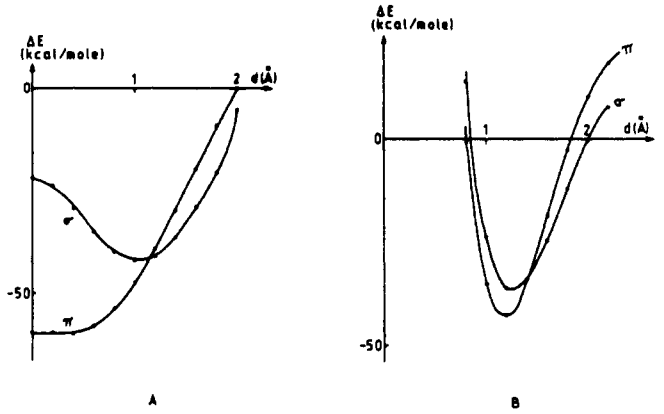

Figure 12. Plots of the change in energy (in kcal mol^{-1}) of the $(Cu^+)_2O_2$ as the distance between the Cu^+–Cu^+ and O–O centers (*d*) is varied: (a) the side-on approach of dioxygen as depicted by **27** and (b) the end-on approach of dioxygen as depicted by **26**. See text for further details. (Reprinted from ref 41. Copyright 1991 American Chemical Society.)

comprised 16 orbitals, 10 from copper (3d, 4s and 4p orbitals) and 6 from dioxygen (the valence orbitals shown in Figure 3). Single reference configurations were used for each calculation (obtained by the excitation of one electron from the copper 3d HOMO to the copper 3d LUMO). The energies of the closed-shell singlet states are lower in energy than either of the open shell states, which is in agreement with the experimental observation that these complexes are diamagnetic.[42]

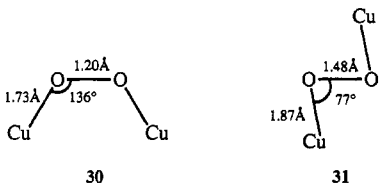

Following these SCF-CI calculations these authors reoptimized the ground-state singlet and open-shell singlet and triplet states using ROHF-GVB methods. The results of these and the subsequent CI calculations using these reference states are given in Table 4. Analysis of this open-shell singlet, which is only a slightly higher in energy (by 0.0005 au) than the closed-shell singlet, showed that the spin-paired electrons were found to reside on one copper atom, corresponding to contributions from the ionic Cu^{2+}–Cu^0 structures—a description which is not obtained explicitly from the closed-shell calculations. Although the exact orbital structure remains unclear, the result that a singlet state *trans* isomer is most stable, is in agreement with those obtained from SCF-Xα-SW calculations.[36]

An important consequence of the fact that the lowest energy isomer is *trans* and closed shell is that antiferromagnetic coupling of the unpaired electrons occurs through the single dioxygen ligand, and an extra bridging ligand, as in **32**, is not required. Finally, the results obtained for these bare $[Cu_2O_2]^{2+}$ molecules[41] also shows that the addition of ligands does not affect dioxygen complexation but does help screen the replusions between the cationic copper centers.

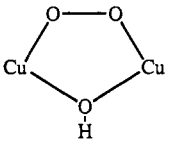

32

The variation in energy with changing dioxygen orientation was also studied using EHMO theory[43] (Table 1, entry 9) using the model complex **33** which is similar to **28** although each copper center has three ammonia ligands attached to it, *i.e.*, the molecule is now $[\{(NH_3)_3Cu\}_2O_2]^{2+}$. The curves plotted in Figure 13 show that the minimum energy geometry of **33** is obtained when the Cu–O_2–Cu unit is planar, which is in agreement with the experimental molecular structure of a model complex, $[Cu(HB(3,5\text{-}i\text{-}Pr_2pz)_3)]_2(O_2)$.[43] This result is also in agreement with the results discussed above for the bare Cu_2O_2 complexes.[41] A calculation where each oxygen atom is connected to only one copper atom (*i.e.*, the μ-η^1:η^1 O_2 structure **34**) was higher in energy than the μ-η^2:η^2 O_2 geometry (**33**) lending further support for the dibridging structure.

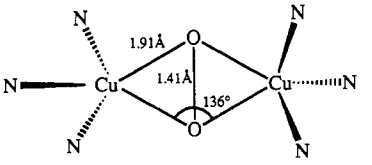

33

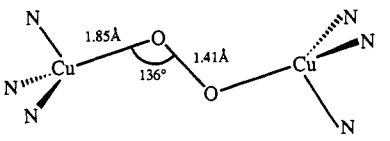

34

EHMO calculations of the complex $[\{(NH_3)_4Cu\}_2O_2]^{2+}$ (**35**), in which each copper atom has a trigonal bipyramidal coordination environment, were also performed.[43] This geometry was lower in energy than a dibridged structure since the latter would result in an unfavorable geometry on the basis of two edge-sharing octahedra. The HOMO–LUMO gap of **35** (0.275 eV) was found to be smaller than that of **33** (0.883 eV, the complex for which this is a model is known to be diamagnetic) but larger than that of **34** (0.089 eV, predicted to be paramagnetic). Since the value of the HOMO–LUMO energy is intermediate between these

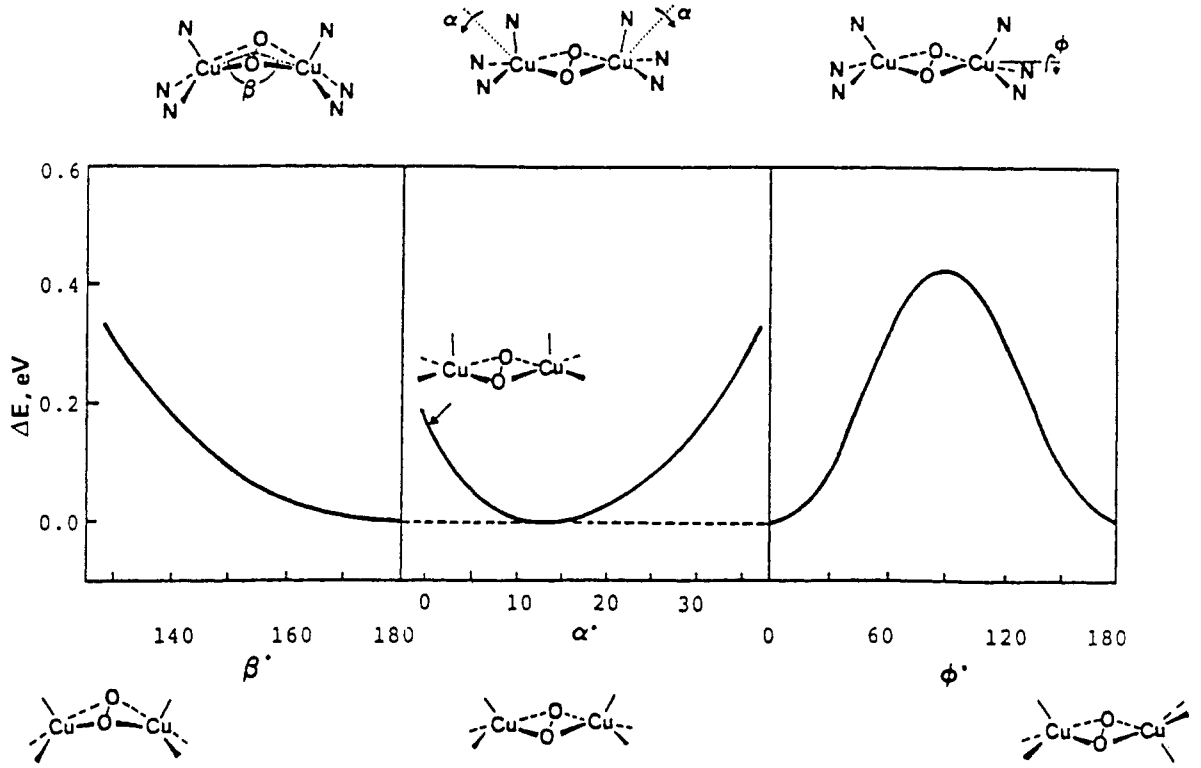

Figure 13. A plot of the change in potential energy with changing geometry of the $[\{(NH_3)_3Cu\}_2(\mu\text{-}\eta^2\text{:}\eta^2\ O_2)]^+$ complex. Variables are defined above each curve. (Reprinted from ref 43. Copyright 1992 American Chemical Society.)

values, it was not possible to designate **35** with certainty as either para- or diamagnetic, although the complex for which **35** is a model, $[Cu(N(CH_2Py)_3]_2(O_2)$, was observed to be diamagnetic.[43]

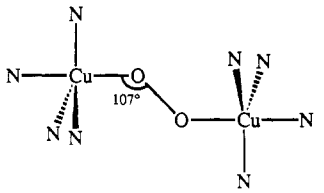

35

A model hemocyanin complex with the general formula $[\{Cu(Im)_3\}_2O_2]^{2+}$ was also examined using EHMO theory[44] (Table 1, entry 10). Two different geometries were considered, the eclipsed hemocyanin (Hc) geometry **36** and the staggered standard average (Sa) geometry **37**. In both complexes the oxygen–oxygen distance was fixed at 1.48 Å, the copper–nitrogen distances at 1.9 and 2.4 Å (these more distant nitrogen atoms, which belong to the coordinated imidazole ligands, are denoted N′ in **36** and **37**), and the copper–copper distances were 3.42 Å in the Hc model and 3.7 Å in the Sa model. The copper–copper–nitrogen angle in the Sa model was fixed at 110°.

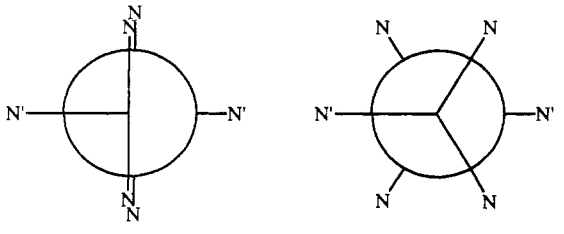

36 37

The lowest energy geometries were calculated when the copper–oxygen and copper–nitrogen planes were perpendicular to each other, *i.e.*, for a dihedral angle between the CuN′ and CuO planes, α, of 90° (see **38**). The difference in energy between the α = 90° and α = 0° geometries for the Hc and Sa complexes is 32 and 8 kcal mol^{-1}, respectively.

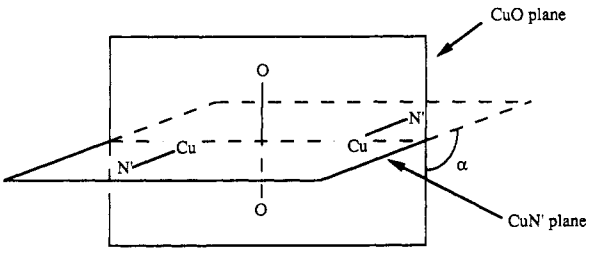

38

These energy differences were explained in MO terms by examining the orbital overlap of the copper and dioxygen orbitals. When α = 90° the sum and difference of the copper orbitals of the Cu–N′ fragment, shown by **39**, interact with the antibonding orbitals of the dioxygen ligand. The sum of the orbitals depicted by **39** interacts with the dioxygen π_g^a orbital, as shown in **40**, and the difference with the dioxygen $3\sigma_u$ orbital, shown in **41**. When α = 0°, the copper orbitals in the Cu–N′–N′ plane, **42**, interact in a similar fashion, although there is less orbital overlap in this case resulting in the lower energy α = 90° geometry. Thus, electron density is transferred from both the dioxygen π_g^a orbital and the copper atom and into the antibonding $3\sigma_u$ orbital. This explanation of the copper–oxygen bonding is similar to that obtained from SCF-Xα-SW calculations on similar dicopper–dioxygen model complexes.[36]

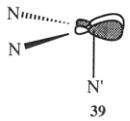

39

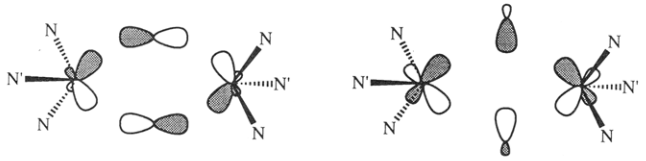

40 41

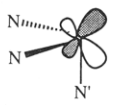

42

The mechanism by which proton binding occurs in these model complexes was also examined by the calculation of electrostatic potential maps, shown in Figure 14. A well close to the dioxygen ligand is deeper than that obtained for free dioxygen by 2 orders of magnitude, indicating that this may provide the driving force for the transfer of a proton from a phenol molecule to the bound dioxygen. Although the molecule is formally dipositive, the transfer of a proton is possible because the Im ligands help reduce the amount of positive charge on the copper atoms.

The effect of rotating of Im ligands was also examined in these EHMO calculations. Of significance was the result that the well depth for the Sa model increased relative to that of the Hc model. Thus ligand orientation may help explain the functional differences between tyrosinase, which acts as an oxidizer, and hemocyanin, which acts as a dioxygen carrier.

The final aspect of the Hc and Sa models studied was the effect of varying the longer Cu–N′ distance. The $\alpha = 90°$ orientation was most stable for all values of this distance, with decreases in both well-depth and the size of the proton-attracting region. These have the effect of decreasing the tyrosinase-like character of the model.

Finally, Xα-SW calculations[45] of the model Cu(O_2) molecule (Table 1, entry 11) in which the dioxygen ligand is bound side on to copper, predict that the ground state is $^2B_2$. Here, one electron is transferred to the π_g^a orbital to make a superoxide bound to a Cu^+. The unpaired electron is mainly in the π_g^s orbital which is delocalized into a copper 3d orbital.

The majority of the calculations discussed in this section was complicated by the lack of certainty surrounding the exact nature of the active sites responsible for the binding of dioxygen to copper in biological systems, although the side-on bridging structure for oxyhemocyanin has recently been established.[46] In addition, the fact that these sites contain two copper atoms increases the amount of computation required, and thus, limits the types of calculation that can be attempted. It is encouraging to find, however, that the large CI calculations for the naked $[Cu_2O_2]^{2+}$ molecules reproduce essentially the same gross geometrical and spectroscopic features as the SCF-Xα-SW and EHMO calculations. The extension of CI, as well as SCF-Xα-SW, calculations to include ligands closer to those anticipated in real molecules, will help in the understanding of the exact nature of the active sites in copper–dioxygen complexes.

IV. Other Metal–Dioxygen Complexes

Several studies of dioxygen complexes, not directly related to the bioinorganic systems discussed above, have also been published. Interest in these complexes arises from their relation to catalysis and a general desire to understand the bonding of end- and side-on dioxygen.

The relative stabilities of the d^6 $[M^{III}O_2(PH_3)_4]^+$ (M = Co, Rh, and Ir) complexes (**43**) were studied using the SCF-Xα-SW method[47] (Table 1, entry 12). For each

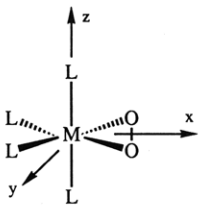

43

of the complexes the doubly occupied d orbitals are the d_{yz}, d_{xz}, and $d_{x^2-y^2}$ leaving the d_{xy} and d_{z^2} unoccupied. The authors attribute the metal–phosphorus bonding to the overlap of the phosphorus lone pairs with the vacant d_{xy} (equatorial plane) and d_{z^2} (axial plane) and the metal–oxygen bonding to overlap between the π_g^s orbital and the metal p_y orbitals. This may be explained in terms of the ordering of orbital energies since PH_3 lone pair < oxygen π_g and metal–d_{xy} < metal–p_y. Plots of the π_g^s MO for the cobalt complex with and without the inclusion of the cobalt p orbital are given in Figure 15. In our view these plots suggest that the phosphorus lone pairs are also strongly involved in interactions with the p_y orbital and that d_{xy}–p_y mixing is also very important for the O_2 bonding. When the cobalt p orbitals are removed the largest changes occur on the cobalt–phosphorus side of the plot where an extra contour (of magnitude four) now appears between the metal and phosphorus atoms while on the oxygen atoms these contours are unchanged.

The calculated relative energies of these complexes were obtained from the respective enthalpies of formation and gave Co (0.0 kcal mol^{-1}) << Ir (114.2 kcal mol^{-1}) < Rh (123.8 kcal mol^{-1}). This ordering is consistent with the experimental results,[48] obtained from the rates of reaction between dioxygen and the d^8 square planar ML_4 complexes. The relative stabilities of the iridium and rhodium complexes are similar, consistent with the experimental results,[48] but are not quantitatively correct. In order to reproduce the experimentally observed enthalpies of formation it may be necessary to include corrections for both electron correlation and full relativistic effects.[43]

The D_{2d} dodecahedral $[M(O_2)_4]^{n-}$ tetraperoxides (**44**) are perhaps the simplest complexes containing side-on-coordinated dioxygen ligands. The electronic structures of the Cr(V), Mo(VI), and Nb(V) complexes of this type were calculated using the SCF-MS-Xα method with bond lengths and angles obtained from crystallographic data[49] (Table 1, entry 13).

Singlet ground states ($^1A_1$) were obtained for the molybdenum and niobium complexes while the ground

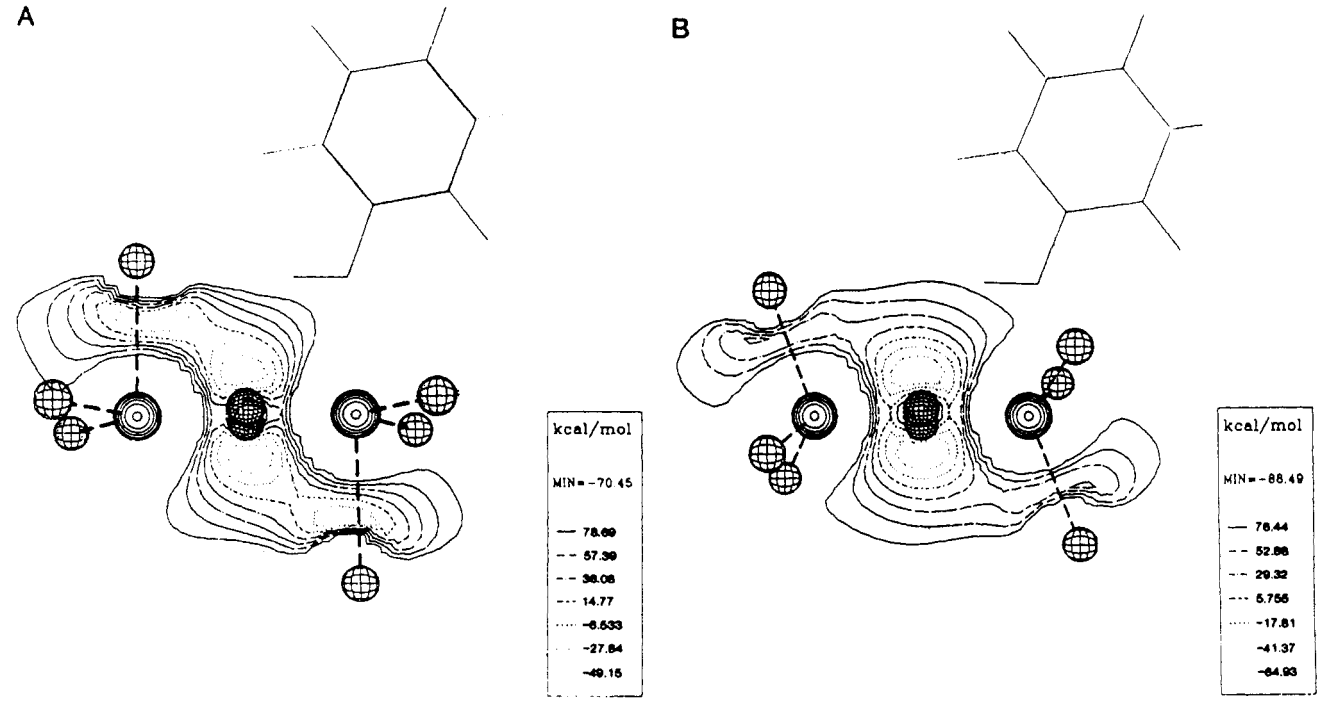

Figure 14. Molecular electrostatic potential maps in the CuN′ plane of the optimized $[(CuIm_3)_2O_2]^{2+}$ complexes: (a) for the Hc geometry, and (b) for the Sa geometry. An approaching phenol ligand is also shown. (Reprinted from ref 41. Copyright 1991 American Chemical Society.)

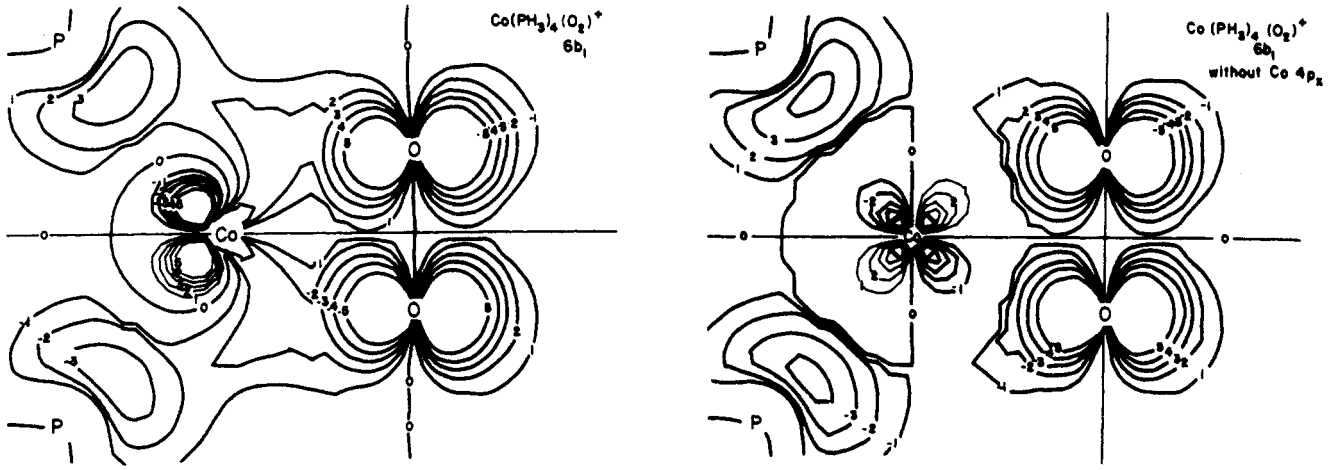

Figure 15. Plots of the π_g^* orbital for the $[Co(PH_3)_4O_2)]^+$ complex: (a) with the cobalt 4p orbital included and (b) with the cobalt 4p orbital excluded in order to show the influence of the interactions with this orbital to cobalt–dioxygen binding. (Reprinted from ref 47. Copyright 1982 American Chemical Society.)

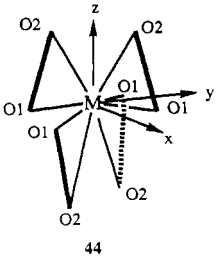

44

state of the chromium complex is $^2B_1$, in which the lowest energy d orbital is occupied. The ordering of the d orbitals in increasing energy is $d_{x^2-y^2} < d_{z^2} \approx d_{xz}, d_{yz} < d_{xy}$, all of which are unoccupied for the niobium and molybdenum complexes. An interesting feature of these complexes is the fact that there are two different metal–oxygen bond lengths (*i.e.*, the M-O1 bond length is longer than the M–O2 bond length in **44**). The 7e, $6a_1$, 6e, and $5b_2$ MO's are shown in Figure 16 and these may be used to account for this difference in bond length. The $6a_1$ and $5b_2$ orbitals interact with both O1 and O2 in much the same way while the 7e and 6e orbitals are both more strongly M–O2 σ bonding. Although the 7e orbital is weakly M-O1 bonding, the 6e orbital is strongly M-O1 antibonding. As this is the only difference in the description of the M–O bonding in these complexes, it is the relative strength of this antibonding interaction which determines how much longer the M–O1 bond will be compared to the M–O2 bond.[49]

Of these tetrakisperoxo complexes the largest donation of charge from ligand to metal occurs in the molybdenum complex because of its high oxidation state. The lower lying molybdenum orbitals also interact more strongly with the O_2 π_u bonding orbitals. From this result it may be concluded that binding of dioxygen to molybdenum weakens the O–O bond more

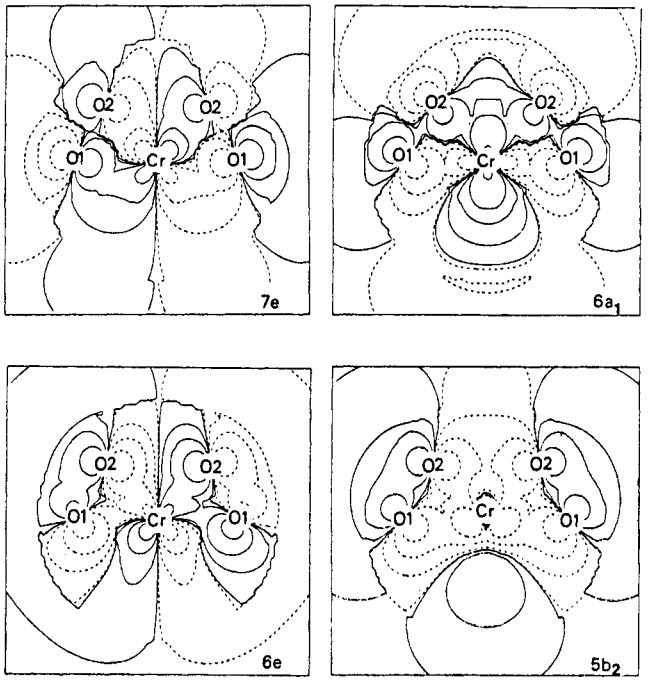

Figure 16. The MO's important to the metal–oxygen binding in $[Cr(O_2)_4]^{3-}$. (Reprinted from ref 49. Copyright 1984 American Chemical Society.)

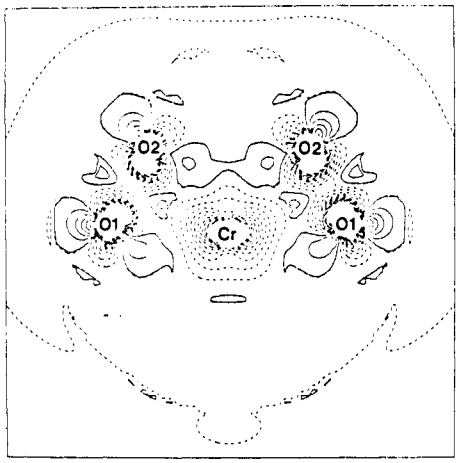

Figure 17. A deformation density map calculated for the D_{2d} dodecahedral $[Cr(O_2)_4]^{3-}$ complex, plotted in one of the trapezoidal planes formed by a $Cr(O_2)_2$ subunit. Contour values are in steps of 0.1 eÅ^{-3} with solid lines denoting positive values and dashed lines negative. (Reprinted from ref 49. Copyright 1984 American Chemical Society.)

than in the other complexes enabling the molybdenum complex to undergo nucleophilic attack which results in cleavage of the dioxygen bond, *i.e.*, ligand to metal charge donation results in a somewhat electrophilic dioxygen ligand. Correspondingly, the niobium complex, which has greater charge on the dioxygen ligand, does not react in the same way with nucleophiles.[49]

The deformation density distribution for the $[Cr(O_2)_4]^{3-}$ complex was also calculated and is shown in Figure 17. This was obtained by subtracting from the calculated electron density, a promolecule constructed from individual atoms unperturbed by bonding. In this case the promolecule consisted of Cr^0 (with a $3d^6$ valence electron configuration) and eight $O^{-0.375}$ (each with a $2s^2\ 2p_x^{1.4583}2p_y^{1.4583}2p_z^{1.4583}$ valence electron configuration). Interesting features of this map are the regions of increased charge density between the O2 atoms and the regions near the oxygen atoms due to the lone pairs. This map could provide an excellent test for the SCF-MS-Xα method as it can, in principle, be compared to one constructed from an experimental determination of the charge-density distribution.

Various geometries of the complex $Ni(O_2)(N_2)$ were studied[50] at the RHF level using basis sets of double-ζ quality (Table 1, entry 14). The purpose of these calculations was to study the preference for the side-on or end-on coordination of the dioxygen and dinitrogen ligands to nickel. The geometry with side-on dioxygen and end-on dinitrogen **45** was found to be more stable than the other isomers studied **46** and **47**. This result agrees with the geometry proposed on the basis of infrared measurements.[51] The preference for side-on dioxygen and end-on dinitrogen was also expected from MO index calculations at the CNDO/2 level, which predicted that the dioxygen ligand binds side on due to better donor properties than the dinitrogen ligand.[52]

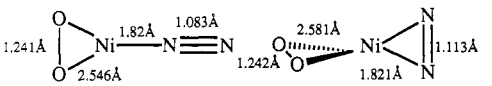

45 46

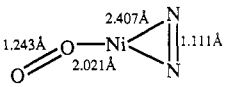

47

Optimization of **45** and **46** with the reduction of symmetry from C_{2v} to C_s resulted in slightly different geometries **48** and **49**, although the energy of **45** was reported to be almost the same as **48**.[50] Infrared absorption bands were also calculated; those for O–O stretching were overestimated while those for N–N were similar to those observed. As we have seen in the calculations discussed above, further study by methods which include electron correlation should be performed if a more accurate description of these molecules is desired.

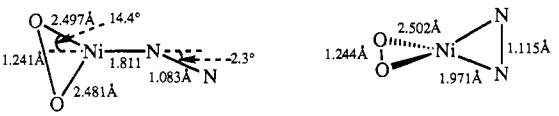

48 49

The reactivity of metal–dioxygen complexes with organic substrates is an important area of synthetic chemistry. Early transition metal–dioxygen complexes react with alkenes to form epoxides[53] (**50**), although the mechanism by which this reaction occurs, either via attachment of the alkene to the coordinated dioxygen ligand[54] or via coordination of the alkene to the metal center,[55] is still a matter of debate as it is for the oxidation of sulfides.[56] Late transition metal complexes, on the other hand, react with ketones and aldehydes to form five-membered peroxometallocyclic adducts[57] (**51**). Calculations of dioxygen complexes of early and late transition metals (**52** and **53**, respectively) are then important in the understanding of how and why these different reactions take place.

In order to compare the differences in reactivity of early and late transition metal complexes the peroxotitanium(IV) 2,6-pyridinedicarboxylate (**52**) and per-

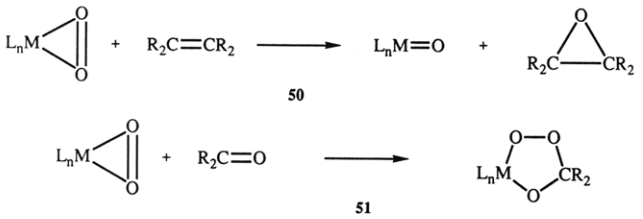

50

51

oxonickel bis(methlyisocyanate) (**53**) complexes were studied.[58] The electronic structures of these molecules were calculated at the HF level using triple-ζ basis sets to describe the metal atoms and double-ζ the other atoms (Table 1, entry 15). Because these are both rather large molecules, observed geometrical parameters were used in the calculations and for each molecule both open and closed shell states were considered.

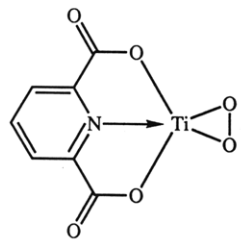

52

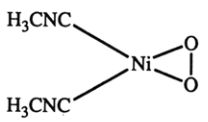

53

A closed-shell $^1A_1$ ground state was obtained for the titanium complex **52** and is lower in energy than the lowest energy open-shell state by several hundred kilocalories per mole. The two important orbital interactions are the π type (**54**), between the titanium d_{yz} and dioxygen π_g^s orbitals and the δ type (**55**), which involve the titanium d_{xy} and dioxygen π_g^a orbitals.

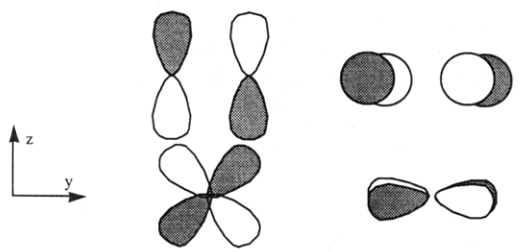

54 55

In contrast to the result for the titanium complex, an open-shell ground state was found for the nickel complex, **53**, and the difference in energy between the ground $^3B_2$ state and the singlet state was predicted to be several hundred kilocalories per mole. This result is unexpected since the d^8 square planar complex **56** was observed to be diamagnetic,[59] as expected.[60] Furthermore, the highest SOMO in the $^3B_2$ state is a π^* orbital belonging to the methylisocyanate ligand, and not a nickel d orbital.

Since this result disagrees with previously reported experiments[59] and theoretical (INDO-SCF) calculations,[61] we performed calculations for this complex at different levels of theory,[62] using the experimental geometry[63] (**56**) but with the slight modification that the terminal methyl group was replaced by hydrogen on the isocyanate ligand (Table 1, entry 16). Our SCF results for the experimental geometry suggest that a singlet ($^1A_1$) state is lower in energy than the previously calculated $^3B_2$ state described above.[58] A subsequent SCF calculation on a $^3B_1$ states, obtained by occupying the nickel d_{yz} orbital instead of the C–N antibonding π orbital, was found to be of lower energy than the $^1A_1$ state, though by only 0.3 kcal mol^{-1}. MRSDCI calculations suggest that the $^1A_1$ state is the ground state and that the $^3B_1$ state is the first excited state.[62]

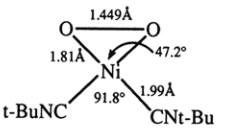

56

The coordination of dioxygen to palladium is also important in homogeneous catalytic oxidation reactions. Although the preferred mode of coordination of dioxygen to palladium has not been established,[64] calculations of several geometries of the monomeric $[Pd(HCO_2)(O_2)]$ complex were performed at the CNDO-S[2] level of theory (Table 1, entry 17). The planar geometry, **57** was lower in energy than both the tetrahedral, **58**, or end on, **59**, isomers by 11.2 and 12.6 kcal mol^{-1} respectively. The stability of **57** over **58** and **59** is presumably a consequence of stronger interactions between a vacant palladium d orbital and the dioxygen π_g^s orbital, in much the same manner as in the nickel complexes, **45–47** discussed above.

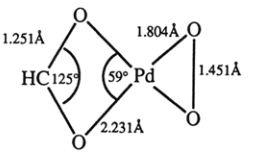

57

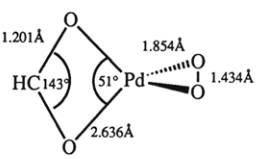

58

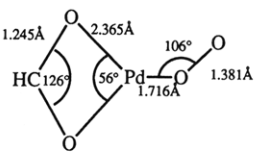

59

The relative stability of isomers of the trimeric palladium species, $[Pd_3(HCO_2)_5(O_2)]$, were also studied, the most stable of which contains the dioxygen ligand bound in the end-on fashion (Figure 18). The change in preference for end-on coordination is a consequence of repulsions between the dioxygen π_g^s orbitals and filled palladium d orbitals. This finding agrees with the known reactivities of mono- and trimeric palladium complexes. Epoxidation reactions involving both mono- and trimeric palladium complexes result in the addition of an oxygen atom to the olefin, with the trimeric species a more reactive participant in alkene epoxidation.

V. Conclusion

All of the studies of the bonding between metals and dioxygen reviewed here reflect the diverse range of chemistry encountered in these systems, and it is clear that the coordination of dioxygen to metals is dependent upon the surrounding ligand environment as well as the type of metal atom. We have seen that CASSCF

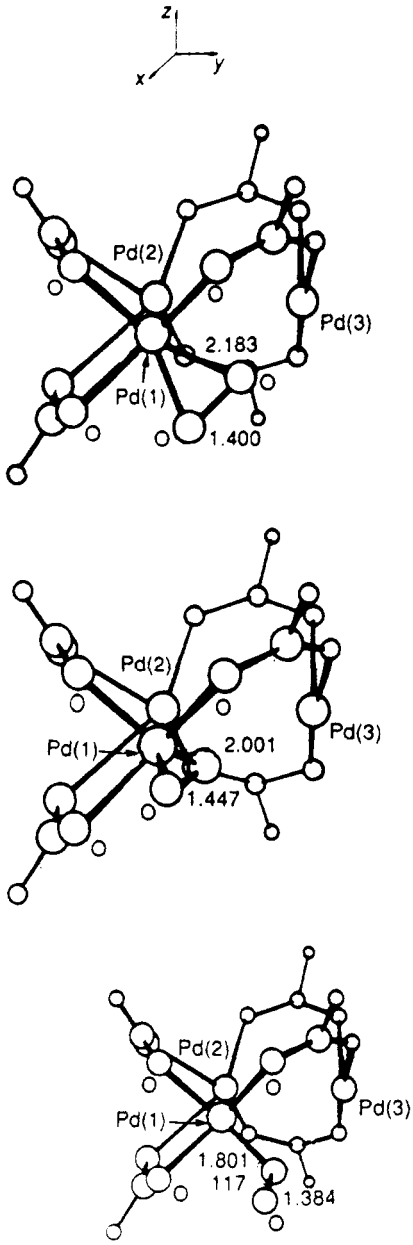

Figure 18. The calculated geometries of three isomers of $[Pd_3(HCO_2)_5(O_2)]$. (top, a) The dioxygen ligand is attached to the palladium atom in a side-on fashion and the four oxygen atoms attached to the palladium atom lie in the same plane. This isomer is 32.1 kcal mol^{-1} above the lowest energy isomer. (middle, b) The dioxygen ligand is attached to the palladium atom in a side-on fashion also, but is perpendicular to the plane formed by the other oxygen atoms attached to the palladium atom. This isomer is 12.1 kcal mol^{-1} above the lowest energy isomer. (bottom, c) The lowest energy isomer. The dioxygen ligand is coordinated to the palladium atom in an end-on manner. (Reprinted from ref 64. Copyright 1990 Chemical Society of London.)

or MCSCF calculations followed by MRSDCI can provide accurate descriptions of energies for the various isomers and states of metal–dioxygen complexes. While relatively expensive, the fact that these methods provide meaningful chemical descriptions, coupled with the continuing increase in computational power, suggests that the study of reaction mechanisms involving metal dioxygen complexes should be pursued with these accurate methods.

Proper description of the bonding interactions in these systems is important to the understanding of the biochemical uptake of oxygen, the synthesis of oxygen-containing organic molecules, and catalytic processes which utilize dioxygen complexation. Consequently, metal–dioxygen chemistry still represents a challenge to the theoretical chemist—one which has tangible goals.

VI. Abbreviations

CASSCF	complete active space self-consistent field
CI	configuration interaction
CISD	configuration interaction including all single and double excitations
CNDO	complete neglect of differential overlap
EHMO	extended Hückel molecular orbital
ESR	electron spin resonance
GMO	generalized molecular orbital
GVB	generalized valence bond
HF	Hartree–Fock
HOMO	highest occupied molecular orbital
Im	imidazole
INDO	incomplete neglect of differential overlap
L	the ligand axial to dioxygen in octahedral complexes
LCAO	linear combination of atomic orbitals
LUMO	lowest unoccupied molecular orbital
MCSCF	multiple configuration self-consistent field
MO	molecular orbital
MS	multiple scattering
MWH	Mulliken–Wolfsberg–Helmholtz
MRSDCI	multiple reference configuration interaction including all single and double excitations
P	porphyrin or model ligand used in a calculation
RHF	restricted Hartree–Fock
ROHF	restricted open-shell Hartree–Fock
SCF	self-consistent field
SOMO	singly occupied molecular orbital
SW	scattered wave
QS	quadrapole splitting
UHF	unrestricted Hartree–Fock
VB	valence bond

Acknowledgments. Financial support from the Robert A. Welch Foundation, grant no. A-648, is gratefully acknowledged. We would like to thank Profs. E. I. Solomon, C. Giessner-Prettre, J. Maddulano, K. A. Jørgensen, and H. Kashiwagi for pre- and reprints and Dr Z. Lin for many useful comments and suggestions during the preparation of the manuscript. We also thank the referees for their helpful suggestions and comments.

VII. References

(1) Dedieu, A.; Rohmer, M.-M.; Viellard, A. *Adv. Quant. Chem.* **1982**, *16*, 43–95.
(2) Loew, G. H. In *Iron Porphyrins: Part One*; Lever, A. B. P., Gray, H. B. Eds.; Addison-Wesley: Massachusetts, 1983; pp 1–87.
(3) Hall, M. B. In *Oxygen Complexes and Oxygen Activation by Transition Metals*; Martell, A. E., Sawyer, D. T., Eds.; Plenum: New York, 1988; pp 3–16.
(4) Smith, T. D.; Pilbrow, J. R. *Coord. Chem. Rev.* **1981**, *39*, 295–383.
(5) Gubelmann, M. H.; Williams, A. F. *Struct. Bonding* **1983**, *55*, 1–65.
(6) Boča, R. *Coord. Chem. Rev.* **1983**, *50*, 1–72.
(7) Dioxygen complexes of B, Al, and Ga were prepared and subsequently studied at the semiempirical level by Alexandrox et al. (Alexandrov, Yu. A.; Vyshinskii, N. N.; Kokorev, V. N.; Alferov, V. A.; Chikinova, N. V.; Makin, G. I. *J. Organomet. Chem.* **1987**, *332*, 259–269).
(8) See for example: (a) Levine, I. N. *Quantum Chemistry*, 4th ed.; Prentice Hall: New Jersey, 1991. (b) Szabo, A.; Ostlund, N. S. *Modern Quantum Chemistry*, 1st ed. (Revised); McGraw-Hill: New York, 1989.
(9) Summerville, D. A.; Jones, R. D.; Hoffman, B. M.; Basolo, F. *J. Chem. Educ.* **1979**, *56*, 157–162.

(10) Drago, R. S. *Inorg. Chem.* **1979**, *18*, 1408–1410.
(11) Pauling, L.; Coryell, C. D. *Proc. Natl. Acad. Sci. U.S.A.* **1936**, *22*, 210–216.
(12) Pauling, L. *Nature* **1964**, *203*, 182–183.
(13) Weiss, J. J. *Nature* **1964**, *202*, 83–84.
(14) See for example: Bade, D.; Parak, F. Z. *Naturforsch.* **1978**, *33c*, 488–494.
(15) McClure, D. S. *Radiation Res. Suppl.* **1960**, *2*, 218–242.
(16) (a) Harcourt, R. D. *Int. J. Quantum Chem.* **1971**, *5*, 479–495. Harcourt, R. D. *J. Inorg. Nucl. Chem.* **1977**, *39*, 243–247. (c) Harcourt, R. D. Qualitative Valence-Bond Descriptions of Electron-Rich Molecules: Pauling "3-Electron Bonds" and "Increased-Valence Theory". *Lecture Notes in Chemistry*; Springer Verlag: Berlin, 1982, Vol. 30, p 200. (d) Harcourt, R. D. *Chem. Phys. Lett.* **1990**, *167*, 374–377.
(17) Goddard, W. A., III; Olafson, B. D. *Proc. Natl. Acad. Sci. U.S.A.* **1975**, *72*, 2335–2339.
(18) Olafson, B. D.; Goddard, W. A., III *Proc. Natl. Acad. Sci. U.S.A.* **1977**, *74*, 1315–1319.
(19) A bent FeO_2 geometry was first established on the basis of the X-ray crystal structure of the dioxygen adduct of (1-methylimidazolyl)-*meso*-tetrakis(α,α,α,α-o-pivalamidophenyl)porphinatoiron-(II) by Jameson et al. (Jameson, G. B.; Rodley, G. A.; Robinson, W. T.; Gagne, R. R.; Reed, C. A.; Collman, J. P. *Inorg. Chem.* **1978**, *17*, 850–857).
(20) Griffith, J. S. *Proc. R. Soc. London, Ser. A* **1956**, *235*, 23–36.
(21) Gray, H. B. *Adv. Chem. Ser.* **1971**, *100*, 365–389.
(22) Newton, J. E.; Hall, M. B. *Inorg. Chem.* **1984**, *23*, 4627–4632.
(23) (a) Cerdonio, M.; Congui-Castellano, A.; Mogno, F.; Pispisa, B.; Romani, G. L.; Vitale, S. *Proc. Natl. Acad. Sci. U.S.A.* **1977**, *74*, 398–400. (b) Cerdonio, M.; Congui-Castellano, A.; Celabrese, L.; Morante, S.; Pispisa, B.; Vitale, S. *Proc. Natl. Acad. Sci. U.S.A.* **1978**, *75*, 4916–4919.
(24) Pauling, L. *Proc. Natl. Acad. Sci. U.S.A.* **1977**, *74*, 2612.
(25) Rohmer, M.-M. In *Quantum Chemistry: The Challenge of Transition Metals and Coordination Chemistry*; Viellard, A., Ed.; NATO ASI Series C: Mathematical and Physical Sciences; Reidel: Holland, 1986; Vol. 176, pp 377–390.
(26) (a) Nozawa, T.; Hatano, M.; Nagashima, U.; Obara, S.; Kashiwaga, H. *Bull. Chem. Sco. Jpn.* **1983**, *56*, 1721–1727. (b) Kashiwagi, H. In *Biomolecules*; Nagata, C., *et al.*, Eds.; Japan Sci. Soc. Press, Tokyo, 1985; pp 31–50.
(27) Yamamoto, S.; Kashiwagi, H. *Chem. Phys. Lett.* **1989**, *161*, 85–89.
(28) Yamamoto, S.; Kashiwagi, H. *Chem. Phys. Lett.* **1993**, *205*, 306–312.
(29) Yamaguchi, K.; Takahara, Y.; Fueno, T. In *The Role of Oxygen in Chemistry and Biochemistry*; Ando, W.; Moro-oka, Y., Eds.; Elsevier: Amsterdam, 1988.
(30) Stavrov, S. S.; Dikusar, I. P.; Bersuker, I. B. *Mol. Biol.* **1987**, *21*, 282–290.
(31) Bertran, J.; Ruiz-López, M. F.; Rinaldi, D. *J. Mol. Struct., THEOCHEM* **1991**, *232*, 337–347.
(32) (a) Weschler, C. J.; Hoffman, B. M.; Basolo, F. *J. Am. Chem. Soc.* **1975**, *97*, 5278–5280. (b) Hoffman, B. M.; Weschler, C. J.; Basolo, F. *J. Am. Chem. Soc.* **1976**, *98*, 5473–5482. (c) Hoffman, B. M.; Szymanski, T.; Brown, T. G.; Basolo, F. *J. Am. Chem. Soc.* **1978**, *100*, 7253–7259.
(33) Urban, M. W.; Nakamoto, K.; Basolo, F. *Inorg. Chem.* **1982**, *21*, 3406–3408.
(34) Newton, J. E.; Hall, M. B. *Inorg. Chem.* **1985**, *24*, 2573–2577.
(35) Cotton, F. A.; Wilkinson, G. *Advanced Inorganic Chemistry*, 5th ed.; Wiley-Interscience: New York, 1988; p 1367.
(36) Ross, P. K.; Solomon, E. I. *J. Am. Chem. Soc.* **1990**, *112*, 5871–5872.
(37) Solomon, E. I.; Baldwin, M. J.; Ross, P. K.; Tuczek, F. In *Dioxygen Activation and Homogeneous Catalytic Oxidation*; Simándi, L. I., Ed.; Elsevier Science Publishers B.V.: Amsterdam, 1991; pp 357–366.
(38) Ross, P. K.; Solomon, E. I. *J. Am. Chem. Soc.* **1991**, *113*, 3246–3259.
(39) Baldwin, M. J.; Ross, P. K.; Pate, J. E.; Tyeklar, Z.; Karlin, K. D.; Solomon, E. I. *J. Am. Chem. Soc.* **1991**, *113*, 8671–8679.
(40) Solomon, E. I.; Tuczek, F.; Root, D. E.; Brown, C. A. *Chem. Rev.* This issue.
(41) Maddaluno, J.; Giessner-Prettre, C. *Inorg. Chem.* **1991**, *30*, 3439–3445.
(42) Solomon, E. I. *Pure Appl. Chem.* **1983**, *55*, 1069–1088.
(43) Kitajimi, N.; Fujisawa, K.; Fujimoto, C.; Moro-oka, Y.; Hashimoto, S.; Kitagawa, T.; Toriumi, K.; Tatsumi, K.; Nakamura, A. *J. Am. Chem. Soc.* **1992**, *114*, 1277–1291.
(44) Eisenstein, O.; Giessner-Prettre, C.; Maddaluno, J.; Stussi, D.; Weber, J. *Arch. Biochem. Biophys.* **1992**, *296*, 247–255.
(45) Mattar, S. M.; Ozin, G. A. *J. Phys. Chem.* **1988**, *92*, 3511–3518.
(46) Ton-That, H.; Magnus, K. *J. Inorg. Biochem.* **1993**, *51*, 65.
(47) Norman, J. G., Jr.; Ryan, P. B. *Inorg. Chem.* **1982**, *21*, 3555–3557.
(48) Vaska, L.; Chen, L. S.; Miller, W. V. *J. Am. Chem. Soc.* **1971**, *93*, 6671–6673.
(49) Roch, M.; Weber, J.; Williams, A. F. *Inorg. Chem.* **1984**, *23*, 4571–4580.
(50) Hori, K.; Asai, Y.; Yamabe, T. *Inorg. Chem.* **1983**, *22*, 3218–3220.
(51) (a) Kozbücher, W. E.; Ozin, G. A. *J. Am. Chem. Soc.* **1975**, *95*, 3790–3792. (b) Ozin, G. A.; Kozbücher, W. E. *J. Am. Chem. Soc.* **1975**, *97*, 3965–3974.
(52) Katsoulos, G. A.; Sigalas, M. P.; Tsipis, C. A. *Inorg. Chim. Acta* **1989**, 255–264.
(53) Sheldon, R. A. In *The Chemistry of Peroxides*; Patai, S., Ed.; Wiley-Interscience: New York, 1983; pp 161–200.
(54) Chong, A. O.; Sharpless, K. B. *J. Org. Chem.* **1977**, *42*, 1587–1590.
(55) Mimoun, H. *J. Mol. Catal.* **1980**, *7*, 1–29.
(56) Kagan, H. B.; Rebiere, F. *Synlett* **1990**, 643–650.
(57) Finn, M. G.; Sharpless, K. B. In *Asymmetric Synthesis*; Morrison, J. D., Ed.; Academic Press: New York, 1986; Vol. 5, pp 247–308.
(58) Jørgensen, K. A.; Swanstrøm, P. *Acta Chem. Scand.* **1992**, *46*, 82–86.
(59) Otsuka, S.; Nakamura, A.; Tatsuno, Y. *J. Am. Chem. Soc.* **1969**, *91*, 6994–6999.
(60) Cotton, F. A.; Wilkinson, G. *Advanced Inorganic Chemistry*, 5th ed.; Wiley-Interscience: New York, 1988; p 747.
(61) Tatsumi, K.; Fueno, T.; Nakamura, A.; Otsuka, S. *Bull. Chem. Soc. Jpn.* **1976**, *49*, 2164–2169.
(62) Bytheway, I.; Hall, M. B. Manuscript in Preparation.
(63) Matsumoto, M.; Nakatsu, N. *Acta Crystallogr.* **1975**, *B31*, 2711–2713.
(64) Filatov, M. J.; Talsi, E. P.; Gritsenko, O. V.; Zhidomirov, G. M.; Zamaraev, K. I. *J. Chem. Soc., Dalton Trans.* **1990**, 3265–3269.